Contemporary Mathematics
https://ojs.wiserpub.com/index.php/CM/

Research Article

Cubic-Quartic Solitons for Gerdjikov-Ivanov Equation with Differential Group Delay in Presence of Multiplicative White Noise

Hanaa A. Eldidamony[1], Taher A. Nofal[2], Yakup Yildirim[3,4*], Ahmed H. Arnous[5], Amer Shaker Mahmood[6], Anjan Biswas[7,8,9,10]

[1]Department of Basic Science, Higher Technological Institute, 10th of Ramadan City, Egypt
[2]Department of Mathematics, College of Science, Taif University, P.O. Box, 11099, Taif, 21944, Saudi Arabia
[3]Department of Computer Engineering, Biruni University, Istanbul, 34010, Turkey
[4]Mathematics Research Center, Near East University, 99138, Nicosia, Cyprus
[5]Department of Engineering Mathematics and Physics, Higher Institute of Engineering, El- Shorouk Academy, Cairo, 11837, Egypt
[6]Department of Medical Laboratory Techniques, Al Nibras University-Iraq, Tikrit, 34001, Iraq
[7]Department of Mathematics & Physics, Grambling State University, Grambling, LA, 71245-2715, USA
[8]Department of Physics and Electronics, Khazar University, Baku, AZ, 1096, Azerbaijan
[9]Department of Applied Sciences, Cross-Border Faculty of Humanities, Economics and Engineering, Dunarea de Jos University of Galati, 111, Domneasca Street, Galati, 800201, Romania
[10]Department of Mathematics and Applied Mathematics, Sefako Makgatho Health Sciences University, Medunsa, 0204, South Africa
E-mail: yyildirim@biruni.edu.tr

Received: 7 April 2025; **Revised:** 3 May 2025; **Accepted:** 20 May 2025

Abstract: This study conducts an in-depth analysis of the Gerdjikov-Ivanov equation under the influence of multiplicative white noise, specifically within the context of birefringent fibers. By employing two advanced techniques-the enhanced direct algebraic method and the innovative projective Riccati equations method-the research uncovers a range of soliton behaviors. The results identify various soliton types, including bright, dark, singular, and straddled solitons. Additionally, the study presents solutions involving Jacobi and Weierstrass doubly periodic functions, which under certain conditions, transition into soliton solutions. This research introduces a novel model, with all solutions representing original contributions to the field. The influence of white noise on these soliton structures is vividly depicted through 3D, 2D, and contour plots, providing visual insights into the dynamics of solitons in the presence of noise disturbances. These graphical representations offer a deeper understanding of soliton behavior within birefringent fibers, thereby advancing the discourse on nonlinear dynamics in optical fibers.

Keywords: soliton solutions, Gerdjikov-Ivanov equation, multiplicative white noise

MSC: 78A60, 81V80

1. Introduction

Optical solitons in birefringent fibers represent a crucial area of interest in photonics, blending theoretical insights with practical implications for telecommunications. These solitons are unique light pulses that travel through fibers, maintaining their shape due to a balance between the medium's nonlinearity and the dispersive effects. Birefringent fibers,

DOI: https://doi.org/10.37256/cm.6320256937

characterized by their dual refractive indices based on the light's polarization direction, offer a nuanced environment for solitons, enhancing their stability and distance over which they can effectively propagate [1–4]. This attribute is crucial for developing advanced optical communication systems, where solitons can be harnessed to transmit data over long distances with reduced loss and interference. The ability to control these solitons opens up possibilities for more efficient and reliable communication technologies, addressing the increasing demands for bandwidth and speed in the digital era. The study and application of solitons in such fibers expand our understanding of light's behavior in complex media, potentially revolutionizing data transmission infrastructure worldwide [5–9].

The advent of cubic-quartic dispersion as a replacement for traditional chromatic dispersion presents a novel paradigm in manipulating optical solitons, heralding a significant leap in optimizing fiber optic transmission. Chromatic dispersion, a phenomenon where different wavelengths of light travel at different speeds within a fiber, often leads to pulse broadening and distortion, adversely affecting the integrity of the transmitted signal. By contrast, cubic-quartic dispersion incorporates higher-order dispersion effects, offering a more sophisticated control over the propagation of solitons [10–13]. This shift from a linear to a nonlinear dispersion model allows for stabilizing soliton dynamics, reducing pulse broadening and enabling data transmission over longer distances without degradation. Moreover, the enhanced control over soliton properties afforded by cubic-quartic dispersion opens up new avenues for high-capacity, ultra-fast optical communication systems. The integration of this advanced dispersion model improves the performance and reliability of existing systems and lays the groundwork for future innovations in optical communication technology [14–19].

The Gerdjikov-Ivanov (GI) equation, a nonlinear mathematical model, is pivotal in analyzing optical solitons, particularly in complex fiber optics environments. This equation, renowned for its ability to describe the evolution of pulses in nonlinear media with higher accuracy, has been further enhanced by adding additional perturbation terms. These terms account for real-world phenomena such as higher-order nonlinearities, gain or loss, and Raman scattering, which were previously oversimplified or neglected. The augmented GI equation provides a more comprehensive framework for predicting the behavior of optical solitons under various perturbations, facilitating the design of more robust and efficient optical communication systems. By incorporating these additional terms, researchers can simulate and understand the impact of complex interactions on soliton dynamics, leading to improved strategies for mitigating distortion and loss. This refined model broadens our understanding of nonlinear optical phenomena and drives the development of advanced fiber optic technologies that cater to the ever-increasing demands for high-speed, long-distance communication [20–29].

This study delves into the perturbed GI equation, focusing on its implications and applications in the context of birefringent optical fibers. The GI equation, a variant of the nonlinear Schrödinger equation, is frequently used in nonlinear optics to model pulse propagation in media where dispersive and nonlinear effects interact. When applied to birefringent fibers, the equation takes on additional significance, as these fibers possess unique characteristics that arise from their two distinct refractive indices. These indices vary depending on the polarization state of the propagating light, creating an anisotropic environment that adds complexity to soliton dynamics. Birefringent fibers are essential in various optical applications due to their ability to support dual polarization modes. This property makes them invaluable in situations requiring precise control of light polarization, such as in telecommunications and sensing technologies. The presence of birefringence means that two orthogonal polarization states of light will propagate at different speeds, leading to intermodal dispersion and complex coupling effects that can influence the stability and behavior of solitons. As such, understanding soliton propagation in birefringent fibers requires addressing how these unique polarization dynamics affect the solutions to the GI equation.

In practical applications, optical fibers operate as interconnected systems, influenced by perturbations and environmental factors that introduce additional complexity. A key focus of this study is to examine the effects of multiplicative white noise as a perturbative factor in the Gerdjikov-Ivanov (GI) equation. Multiplicative noise refers to stochastic fluctuations that vary proportionally with the wave's intensity, introducing randomness into the wave's amplitude, phase, or frequency as it propagates through the fiber. This type of noise serves as a proxy for real-world disturbances, such as thermal fluctuations, mechanical stress, and environmental vibrations that invariably impact fiber systems. By incorporating multiplicative white noise into the GI equation, we aim to simulate realistic conditions and evaluate the stability and resilience of soliton solutions in noisy environments. Unlike additive noise, which imposes a constant level of randomness, multiplicative noise affects the system's parameters based on the wave's characteristics, allowing for a

more dynamic and context-sensitive exploration of soliton behavior. This approach enables us to investigate scenarios where soliton waves are continually modulated by external fluctuations, closely mirroring the challenges faced in long-distance optical transmission and high-precision applications. Consequently, stochastic models are vital for capturing the inherent randomness within real-world systems, setting them apart from deterministic models that assume fixed outcomes. In fields such as biology, economics, and physics, these models offer a nuanced representation of complex phenomena-ranging from genetic drift to market dynamics and particle motion-where uncertainty plays a crucial role in influencing system behavior over time. The Nonlinear Schrödinger Equation (NLSE) and its variants, including the GI equation, exemplify these principles by integrating stochastic elements that account for random fluctuations in wave dynamics. By incorporating stochasticity, these models enhance our understanding of system evolution, accommodating multiple potential trajectories and reinforcing their relevance in explaining the dynamic and nonlinear nature of complex real-world processes.

This study seeks to thoroughly understand the dynamical behavior of solitons governed by the perturbed GI equation within birefringent fibers, considering both fundamental wave characteristics and the influences of noise. Specifically, our objectives include: 1. Investigating Soliton Stability: By simulating the GI equation with varying levels of multiplicative white noise, we examine how solitons respond to noise intensity. Stability analysis focuses on identifying thresholds of noise that solitons can withstand before destabilizing, which is crucial for applications where maintaining wave shape and integrity over long distances is essential. 2. Analyzing Noise-Induced Distortions: Beyond stability, we aim to understand the specific morphological effects that noise introduces. This includes changes in the amplitude, width, and shape of the solitons, particularly under birefringent conditions where the polarization states are sensitive to noise. These findings will provide insights into how solitons may deform or disperse as they propagate, which has implications for maintaining signal quality in fiber-optic systems. 3. Classifying Soliton Types: The GI equation allows for various types of soliton solutions, including bright, dark, and singular solitons. This study categorizes these soliton types based on their noise tolerance and polarization behavior in birefringent fibers. By distinguishing between soliton types, we can identify which forms are best suited to resist noise disturbances, offering potential pathways for optimizing fiber design. 4. Exploring Cross-Phase Modulation and Dispersion Effects: In birefringent fibers, cross-phase modulation and dispersion play a significant role. This study will analyze the interplay of these effects with the noise factor, revealing how polarization-dependent coupling influences soliton characteristics and providing a more comprehensive view of their dynamics. To achieve these objectives, we employ advanced mathematical methods, including stochastic differential equation analysis and numerical simulations. The GI equation with noise is inherently challenging to solve analytically, so a combination of numerical techniques and approximate methods is used to explore its solutions. By simulating different noise intensities and birefringent fiber parameters, we can observe the resulting soliton evolution and make informed conclusions about their behavior in realistic settings.

The findings from this investigation carry substantial relevance for the field of nonlinear optics and its applications in fiber-optic communication. As data transmission demands increase, ensuring signal stability and fidelity in optical fibers under real-world conditions becomes critical. Understanding how solitons react to noise in birefringent fibers can inform fiber design improvements, such as materials or structures that minimize noise impact. Moreover, this study provides a framework for future research into noise effects on nonlinear equations in other contexts, such as biological wave propagation or quantum systems. The interplay of nonlinear dynamics with stochastic perturbations is a universal challenge across many fields, and the methodologies applied here could pave the way for new approaches to managing noise in complex systems. By extending the perturbed GI equation to account for birefringence and noise, this study contributes to the broader understanding of soliton dynamics in optical systems. It lays the groundwork for innovations that enhance optical fiber performance and explores how noise-adaptive soliton solutions might be developed for diverse applications.

The perturbed GI equation with multiplicative white noise, emphasising its relevance to birefringent fibers reads as:

$$iq_t + ia_1 q_{xxx} + b_1 q_{xxxx} + \left(c_1 |q|^4 + d_1 |q|^2 |r|^2 + e_1 |r|^4\right) q + i\left(f_1 q^2 + g_1 r^2\right) q_x^* + \sigma q \frac{dW(t)}{dt}$$

$$= i\left\{\alpha_1 q_x + \beta_1 \left(|q|^2 q\right)_x + \gamma_1 \left(|q|^2\right)_x q\right\},$$

$$ir_t + ia_2 r_{xxx} + b_2 r_{xxxx} + \left(c_2 |r|^4 + d_2 |r|^2 |q|^2 + e_2 |q|^4\right) r + i\left(f_2 r^2 + g_2 q^2\right) r_x^* + \sigma r \frac{dW(t)}{dt}$$

$$= i\left\{\alpha_2 r_x + \beta_2 \left(|r|^2 r\right)_x + \gamma_2 \left(|r|^2\right)_x r\right\}. \tag{1}$$

In this context, the functions $q(x,\ t)$ and $r(x,\ t)$ represent complex-valued wave functions that describe the characteristics and dynamics of wave propagation over space (x) and time (t). These functions encapsulate the amplitude and phase information of the wave, providing a mathematical model for the evolution of wave patterns, where $q(x,\ t)$ and $r(x,\ t)$ could represent two distinct interacting wave modes in a nonlinear medium, such as those in optical fibers or other dispersive media. The initial part of the expression characterizes the evolutionary mechanism of these wave functions. Specifically, the inclusion of i represents the imaginary unit, a fundamental aspect of complex functions that allows for the representation of oscillatory behavior. The imaginary unit is essential in describing phase shifts and rotation within the complex plane, contributing to the oscillatory and propagative features of the wave as it travels through the medium. Several coefficients are defined in this expression to quantify various physical effects influencing the wave's evolution: The coefficients a_l and b_l determine the strength of cubic and quartic dispersion effects, respectively. Dispersion in this context refers to the spreading of the wave packet over time due to the dependence of phase velocity on frequency. Cubic dispersion (a_l) accounts for effects at the third order, whereas quartic dispersion (b_l) pertains to fourth-order dispersion effects. These higher-order dispersive terms become relevant in systems where standard (second-order) dispersion does not sufficiently capture the complex behavior of wave evolution. The coefficient c_l is associated with Self-Phase Modulation (SPM), a nonlinear effect where the phase of the wave is modulated by its own intensity. In SPM, higher-intensity portions of the wave experience a different phase shift than lower-intensity portions, leading to spectral broadening and phase changes that affect the wave's temporal profile. The coefficients d_l and e_l relate to Cross-Phase Modulation (XPM) effects. XPM is a nonlinear interaction where the phase of one wave is modulated by the intensity of another co-propagating wave. In systems with multiple wave modes (such as $q(x,\ t)$ and $r(x,\ t)$), XPM allows for energy transfer and mutual modulation between modes, influencing their respective phases and possibly leading to coupled wave dynamics. The coefficients f_l and g_l quantify additional dispersion effects in the system. These may represent either linear or nonlinear dispersive forces that act to broaden the wave packet, introducing phase shifts that vary with frequency. Dispersion effects are fundamental to wave propagation in dispersive media, as they dictate how different frequency components travel at varying speeds, leading to waveform distortion over time. The parameter σ signifies the strength of multiplicative white noise within the system. Multiplicative noise introduces a stochastic component to the wave function, affecting it proportionally to the wave's intensity. This type of noise simulates real-world perturbations that can vary the properties of the medium unpredictably, leading to fluctuations in wave characteristics and impacting stability. The coefficient α_l is linked to intermodal dispersion, which occurs in systems with multiple wave modes. The Wiener process, denoted as $W(t)$, is a pivotal element in stochastic modeling that encapsulates random fluctuations over time, embodying a continuous and unpredictable development where each increment is independent and normally distributed. In the context of evolutionary dynamics, $W(t)$ effectively represents randomness, such as environmental noise or random perturbations in population size, which impacts system behavior. The significance of $W(t)$ stems from its capability to model phenomena that classical deterministic frameworks cannot adequately address, introducing variability that profoundly shapes the system's trajectory with each time increment. This makes $W(t)$ particularly essential in environments characterized by noise or stochastic shocks, including financial markets and biological processes. By

incorporating $W(t)$, models can better reflect the cumulative impact of random disturbances, thereby enhancing their realism and adaptability in situations dominated by uncertainty and randomness, ultimately offering more nuanced predictions of future behavior. Intermodal dispersion arises from the differential velocities of distinct modes within the medium, leading to a gradual temporal separation between them. This effect can alter the interaction dynamics between the modes, influencing the shape and timing of waveforms as they propagate. The coefficient β_l represents the self-steepening effect, a nonlinear process where the higher-intensity portions of a wave travel slower than lower-intensity portions. This effect creates an asymmetry in the wave profile, typically sharpening the leading edge of the wave and broadening the trailing edge, which can lead to the formation of steep wave fronts or shock-like structures. Finally, the coefficient γ_l is associated with nonlinear dispersion, a phenomenon where dispersion characteristics change with the wave's intensity. Unlike linear dispersion, which uniformly broadens the wave, nonlinear dispersion can lead to complex patterns of wave distortion that depend on intensity variations across the wave. This effect is especially relevant in high-intensity regimes and is often compounded by other nonlinear effects like self-phase modulation and self-steepening. Each of these parameters interacts with the fundamental dispersive and nonlinear aspects of the medium, capturing the combined influences of linear and nonlinear dispersions, noise, intermodal dynamics, and various forms of modulation. These influences collectively govern the behavior of $q(x,\, t)$ and $r(x,\, t)$, providing a detailed framework for understanding wave interactions and the emergence of soliton structures under complex, real-world conditions. The model is thus designed to offer insights into wave stability, propagation characteristics, and the interplay between deterministic and stochastic effects on wave dynamics in nonlinear media.

2. Mathematical analysis

Focusing on waveforms, we aim to derive a solution for Equation (1):

$$q(x,\, t) = U_1(\eta)\, e^{i\phi(x,\, t)},$$

$$r(x,\, t) = U_2(\eta)\, e^{i\phi(x,\, t)}, \tag{2}$$

where

$$\eta = k(x - vt),\ \phi(x,\, t) = -\kappa x + \omega t - \sigma^2 t + \sigma W(t) + \theta_0. \tag{3}$$

Here, the phase term $\phi(x,\, t)$ incorporates both deterministic and stochastic contributions. $-\sigma^2 t$ and $\sigma W(t)$ represent noise effects, with σ^2 influencing deterministic growth/decay and $\sigma W(t)$ introducing random fluctuations modeled by a Wiener process (Brownian motion). $-\kappa x$ and ωt capture spatial and temporal oscillations. $U_l(\eta)$ (for $l = 1,\ 2$) are amplitudes that encode the spatial and temporal structures of each wave component. θ_0 specifies the initial phase offset. k determines the wave width. v represents the velocity of wave propagation. σ governs the strength of multiplicative white noise, introducing stochastic fluctuations in wave behavior. The frequency ω and wave number κ contribute to the oscillatory nature of the solution. η characterizes a traveling wave that depends on both space (x) and time (t), propagating at velocity v. By substituting Eqs. (2) and (3) into Eq. (1), we obtain real and imaginary components separately:

$$U_1\left(-a_1\kappa^3 - \alpha_1\kappa + b_1\kappa^4 + e_1{U_2}^4 - g_1\kappa{U_2}^2 + \sigma^2 - \omega\right) + 3a_1\kappa k^2 U_1'' + b_1 k^4 {U_1}^{(4)}$$

$$-6b_1\kappa^2 k^2 U_1'' + c_1{U_1}^5 - {U_1}^3\left(\beta_1\kappa - d_1{U_2}^2 + f_1\kappa\right) = 0, \tag{4}$$

$$U_2\left(-a_2\kappa^3-\alpha_2\kappa+b_2\kappa^4+e_2{U_1}^4-g_2\kappa{U_1}^2+\sigma^2-\omega\right)+3a_2\kappa k^2U_2''+b_2k^4{U_2}^{(4)}$$

$$-6b_2\kappa^2k^2U_2''+c_2{U_2}^5-{U_2}^3\left(\beta_2\kappa-d_2{U_1}^2+f_2\kappa\right)=0, \tag{5}$$

$$-kU_1'\left(3a_1\kappa^2+\alpha_1-4b_1\kappa^3-g_1{U_2}^2+v\right)+a_1k^3{U_1}^{(3)}-4b_1\kappa k^3{U_1}^{(3)}+k{U_1}^2\left(-3\beta_1-2\gamma_1+f_1\right)U_1'=0, \tag{6}$$

$$-kU_2'\left(3a_2\kappa^2+\alpha_2-4b_2\kappa^3-g_2{U_1}^2+v\right)+a_2k^3{U_2}^{(3)}-4b_2\kappa k^3{U_2}^{(3)}+k{U_2}^2\left(-3\beta_2-2\gamma_2+f_2\right)U_2'=0. \tag{7}$$

Using the balancing principle rule $U_2=\Omega\,U_1$, Eqs. (4)-(7) become:

$$3\kappa k^2\left(a_1-2b_1\kappa\right)U_1''+U_1\left(-a_1\kappa^3-\alpha_1\kappa+b_1\kappa^4+\sigma^2-\omega\right)+b_1k^4{U_1}^{(4)}+{U_1}^5\left(c_1+d_1\Omega^2+e_1\Omega^4\right)$$

$$-\kappa{U_1}^3\left(\beta_1+f_1+g_1\Omega^2\right)=0, \tag{8}$$

$$3\kappa k^2\Omega\left(a_2-2b_2\kappa\right)U_1''+\Omega U_1\left(-a_2\kappa^3-\alpha_2\kappa+b_2\kappa^4+\sigma^2-\omega\right)+b_2k^4\Omega{U_1}^{(4)}+\Omega{U_1}^5\left(c_2\Omega^4+d_2\Omega^2+e_2\right)$$

$$-\kappa\Omega{U_1}^3\left(\beta_2\Omega^2+f_2\Omega^2+g_2\right)=0, \tag{9}$$

$$k^3{U_1}^{(3)}\left(a_1-4b_1\kappa\right)-kU_1'\left(3a_1\kappa^2+\alpha_1-4b_1\kappa^3+v\right)+k{U_1}^2U_1'\left(-3\beta_1-2\gamma_1+f_1+g_1\Omega^2\right)=0, \tag{10}$$

$$k^3\Omega{U_1}^{(3)}\left(a_2-4b_2\kappa\right)-k\Omega U_1'\left(3a_2\kappa^2+\alpha_2-4b_2\kappa^3+v\right)+k\Omega{U_1}^2U_1'\left(-\Omega^2\left(3\beta_2+2\gamma_2\right)+f_2\Omega^2+g_2\right)=0. \tag{11}$$

Eqs. (10) and (11) give the velocity and frequency:

$$v=-3a_1\kappa^2-\alpha_1+4b_1\kappa^3, \tag{12}$$

$$v=-3a_2\kappa^2-\alpha_2+4b_2\kappa^3, \tag{13}$$

and

$$\kappa=\frac{a_l}{4b_l}, \tag{14}$$

with the constraint

$$-3\beta_1-2\gamma_1+f_1+g_1\Omega^2=-\Omega^2\left(3\beta_2+2\gamma_2\right)+f_2\Omega^2+g_2=0. \tag{15}$$

To reduce Equations (8) and (9) to a single equation, we arrive at:

$$-a_1\kappa^3-\alpha_1\kappa+b_1\kappa^4+\sigma^2-\omega=\Omega\left(-a_2\kappa^3-\alpha_2\kappa+b_2\kappa^4+\sigma^2-\omega\right),$$

$$\beta_1+f_1+g_1\Omega^2=\Omega\left(\beta_2\Omega^2+f_2\Omega^2+g_2\right),$$

$$c_1+d_1\Omega^2+e_1\Omega^4=\Omega\left(c_2\Omega^4+d_2\Omega^2+e_2\right),$$

$$b_1=b_2\Omega. \tag{16}$$

Thus, Equation (8) can be simplified to

$$k^2U_1{}^{(4)}(\eta)+\upsilon_4U_1''(\eta)+\upsilon_3U_1(\eta)^5+\upsilon_2U_1(\eta)^3+\upsilon_1U_1(\eta)=0, \tag{17}$$

with

$$\upsilon_1=\frac{-a_1\kappa^3-\alpha_1\kappa+b_1\kappa^4+\sigma^2-\omega}{b_1k^2},$$

$$\upsilon_2=-\frac{\kappa\left(\beta_1+f_1+g_1\Omega^2\right)}{b_1k^2},$$

$$\upsilon_3=\frac{c_1+d_1\Omega^2+e_1\Omega^4}{b_1k^2},$$

$$\upsilon_4=3\kappa\left(\frac{a_1}{b_1}-2\kappa\right). \tag{18}$$

Balancing $U_1{}^{(4)}$ with ${U_1}^5$ in equation (17) exposes $N=1$.

3. Integration algorithms

This section presents a detailed examination of two integration algorithms used to obtain soliton solutions in complex mathematical frameworks. These methods are essential for addressing nonlinear differential equations, particularly those representing soliton dynamics in optical fibers and other nonlinear media. Both techniques are renowned for their robustness in handling intricate mathematical structures and their effectiveness in generating exact or approximate soliton solutions. By providing a comprehensive framework, these algorithms allow researchers to systematically explore and classify various types of soliton solutions, aiding in the analysis of nonlinear phenomena across multiple scientific and engineering domains.

Together, these methods offer a powerful toolkit for researchers in the field of nonlinear dynamics, specifically for studying soliton solutions in complex settings. By providing both exact and approximate solutions, these algorithms allow for a nuanced understanding of soliton dynamics, stability, and behavior under varying conditions, such as

nonlinear dispersion, noise, and perturbative effects. Their applications span across fields such as fluid dynamics, plasma physics, nonlinear optics, and biological wave propagation, where they serve as essential tools for analyzing and controlling nonlinear phenomena. In optical fiber research, for instance, these methods can be instrumental in designing fiber systems that optimize soliton stability and resilience to noise. In fluid dynamics, they enable researchers to simulate shock wave propagation in nonlinear media, while in biology, they help model cellular and neural wave patterns that are inherently nonlinear. By leveraging the strengths of both the enhanced direct algebraic method and the projective Riccati equation method, researchers can construct a diverse set of soliton solutions, gaining insights into the rich dynamics of nonlinear systems and paving the way for future advances in optical communication, signal processing, and material sciences.

Consider a model equation:

$$F(u,\ u_t,\ u_x,\ u_{xx},\ u_{xt},\ ...) = 0. \tag{19}$$

Here, $u = u(x,\ t)$ is waveform. We begin with

$$\eta = k(x - vt),\ u(x,\ t) = U(\eta), \tag{20}$$

where, k signifies the wave width, while the velocity arises from v. As a result, Eq. (19) becomes:

$$F(U,\ kU',\ -vkU',\ k^2U'',\ v^2k^2U'',\ ...) = 0. \tag{21}$$

3.1 *The enhanced direct algebraic scheme*

This method presents a robust and efficient strategy for deriving soliton solutions to nonlinear differential equations through a structured algebraic framework. By constructing polynomial forms that satisfy soliton conditions, it establishes a direct pathway to exact solutions, circumventing complex transformations and the time-consuming process of iterative methods. Its effectiveness is particularly notable for equations involving cubic, quartic, or higher-order nonlinearities, frequently found in advanced optical models and plasma physics, allowing for accurate modeling of intricate phenomena such as soliton propagation. Furthermore, the method's versatility enables the systematic derivation of various types of solitons, accommodating both bright and dark solitons within a unified framework. It is also capable of identifying non-solitary periodic solutions represented by Jacobi elliptic functions, which are crucial for understanding the transition behaviors between periodic and soliton states. This combination of directness, precision, and adaptability makes this method an ideal choice for researchers exploring soliton dynamics in complex systems.

Step 1: Eq. (21) holds [30]:

$$U_1(\eta) = \alpha_0 + \sum_{i=1}^{N} \left[\alpha_i \theta(\eta)^i + \beta_i \theta(\eta)^{-i}\right], \tag{22}$$

with

$$\theta'(\eta)^2 = \sum_{l=0}^{4} \tau_l \theta(\eta)^l,\ \tau_4 \neq 0. \tag{23}$$

Case 1: A bell-shaped soliton with $\tau_2 > 0$ and $\tau_4 < 0$, along with a singular soliton where $\tau_2 > 0$ and $\tau_4 > 0$, emerge when $\tau_0 = \tau_1 = \tau_3 = 0$:

$$\theta(\eta) = \sqrt{-\frac{\tau_2}{\tau_4}}\,\mathrm{sech}\left[\sqrt{\tau_2}\eta\right],\ \tau_2 > 0,\ \tau_4 < 0, \tag{24}$$

$$\theta(\eta) = \sqrt{\frac{\tau_2}{\tau_4}}\,\mathrm{csch}\left[\sqrt{\tau_2}\eta\right],\ \tau_2 > 0,\ \tau_4 > 0. \tag{25}$$

Case 2: When $\tau_0 = \dfrac{\tau_2^2}{4\tau_4}$, $\tau_1 = \tau_3 = 0$, $\tau_2 < 0$ and $\tau_4 > 0$, kink-shaped and singular solitons turn out to be:

$$\theta(\eta) = \sqrt{-\frac{\tau_2}{2\tau_4}}\tanh\left[\sqrt{\frac{-\tau_2}{2}}\eta\right],\ \tau_2 < 0,\ \tau_4 > 0, \tag{26}$$

$$\theta(\eta) = \sqrt{-\frac{\tau_2}{2\tau_4}}\coth\left[\sqrt{\frac{-\tau_2}{2}}\eta\right],\ \tau_2 < 0,\ \tau_4 > 0. \tag{27}$$

Case 3: Jacobi elliptic doubly periodic type solutions emerge when $\tau_1 = 0$ and $\tau_3 = 0$:

$$\theta(\eta) = \pm\sqrt{-\frac{m^2\tau_2}{(2m^2-1)\tau_4}}\,\mathrm{cn}\left(\sqrt{\frac{\tau_2}{(2m^2-1)}}\eta\,\middle|\,m\right);\ \tau_0 = \frac{m^2(1-m^2)\tau_2^2}{(2m^2-1)^2\tau_4}, \tag{28}$$

$$\theta(\eta) = \pm\sqrt{-\frac{m^2\tau_2}{(2-m^2)\tau_4}}\,\mathrm{dn}\left(\sqrt{\frac{\tau_2}{(2-m^2)}}\eta\,\middle|\,m\right);\ \tau_0 = \frac{(1-m^2)\tau_2^2}{(2-m^2)^2\tau_4}, \tag{29}$$

$$\theta(\eta) = \pm\sqrt{-\frac{m^2\tau_2}{(m^2+1)\tau_4}}\,\mathrm{sn}\left(\sqrt{-\frac{\tau_2}{(m^2+1)}}\eta\,\middle|\,m\right);\ \tau_0 = \frac{m^2\tau_2^2}{(m^2+1)^2\tau_4}. \tag{30}$$

Case 4: With $\tau_1 = \tau_3 = 0$, Weierstrass elliptic doubly periodic type solutions are generated as follows:

$$\theta(\eta) = \frac{3\wp'(\eta;\ g_2,\ g_3)}{\sqrt{\tau_4}[6\wp(\eta;\ g_2,\ g_3)+\tau_2]},\ \tau_4 > 0, \tag{31}$$

$$\theta(\eta) = \frac{\sqrt{\tau_0}[6\wp(\eta;\ g_2,\ g_3)+\tau_2]}{3\wp'(\eta;\ g_2,\ g_3)},\ \tau_0 > 0. \tag{32}$$

Here $g_2 = \dfrac{\tau_2^2}{12} + \tau_0\tau_4$ and $g_3 = \dfrac{\tau_2}{216}(36\tau_0\tau_4 - \tau_2^2)$.
Case 5: Straddled solitons emerge when $\tau_0 = \tau_1 = 0$, and $\tau_2 > 0$:

$$\theta(\eta) = \frac{-\tau_2 \operatorname{sech}^2\left[\frac{1}{2}\sqrt{\tau_2}\eta\right]}{\pm 2\sqrt{\tau_2\tau_4}\tanh\left[\frac{1}{2}\sqrt{\tau_2}\eta\right] + \tau_3}, \ \tau_4 > 0, \tag{33}$$

$$\theta(\eta) = \frac{\tau_2 \operatorname{csch}^2\left[\frac{1}{2}\sqrt{\tau_2}\eta\right]}{\pm 2\sqrt{\tau_2\tau_4}\coth\left[\frac{1}{2}\sqrt{\tau_2}\eta\right] + \tau_3}, \ \tau_4 > 0, \tag{34}$$

$$\theta(\eta) = \frac{-\tau_2\tau_3 \operatorname{sech}^2\left[\frac{1}{2}\sqrt{\tau_2}\eta\right]}{\tau_3^2 - \tau_2\tau_4\left(1 - \tanh\left[\frac{1}{2}\sqrt{\tau_2}\eta\right]\right)^2}, \ \tau_3 \neq 0, \tag{35}$$

$$\theta(\eta) = \frac{\tau_2\tau_3 \operatorname{csch}^2\left[\frac{1}{2}\sqrt{\tau_2}\eta\right]}{\tau_3^2 - \tau_2\tau_4\left(1 - \coth\left[\frac{1}{2}\sqrt{\tau_2}\eta\right]\right)^2}, \ \tau_3 \neq 0. \tag{36}$$

Step 2: The parameter N in Eq. (22) is found by balancing the nonlinear terms with the highest-order derivatives in Eq. (21).

Step 3: Eqs. (22) and (23) are substituted into Eq. (21), resulting in a polynomial $\theta(\eta)$. This polynomial is simplified by combining like terms, and the equation is set to zero. Solving the over-determined system that arises from this equation allows us to find the parameters in Eqs. (20) and (22), thereby obtaining the solutions of Eq. (19).

3.2 *The new projective Riccati equations algorithm*

This method is a powerful technique widely utilized in the realm of nonlinear differential equations to derive exact soliton solutions. By harnessing the properties of Riccati-type equations-specific first-order nonlinear differential equations-it adapts to a diverse range of nonlinear scenarios, yielding stable soliton solutions. The method presents several key advantages: first, it systematically transforms complex nonlinear equations into a Riccati-type framework, simplifying the solution process and reducing the complexity of the original equation, thereby facilitating the derivation of exact solutions. Second, it offers versatility in obtaining various soliton structures, including bright, dark, and singular solitons, by varying coefficients and initial conditions. Third, it effectively addresses perturbative systems that are influenced by small fluctuations, such as noise or parametric changes, enabling researchers to analyze the impact of these perturbations on soliton stability and dynamics.

Step 1: Consider the solution of Eq. (21) given by:

$$U_1(\eta) = \alpha_0 + \sum_{i=1}^{N} \psi(\eta)^{i-1}\left[\alpha_i\psi(\eta) + \beta_i\phi(\eta)\right], \tag{37}$$

and

$$\psi'(\eta) = -\psi(\eta)\phi(\eta), \tag{38}$$

$$\phi'(\eta) = 1 - \phi(\eta)^2 - r\psi(\eta),$$

$$\phi(\eta)^2 = 1 - 2r\psi(\eta) + \chi(r)\psi(\eta)^2. \tag{39}$$

Here, α_0, α_i, β_i (where $i = 0, 1, 2, ..., N$), and r are constants, while N is determined based on the balancing principle specified in Eq. (21).

Step 2: As documented in [31, 32], the solutions to Eq. (38) are provided:

Case 1: $\chi(r) = 0$.

$$\psi(\eta) = \frac{1}{2r}\operatorname{sech}^2\left[\frac{\eta}{2}\right], \text{ and } \phi(\eta) = \tanh\left[\frac{\eta}{2}\right]. \tag{40}$$

or

$$\psi(\eta) = -\frac{1}{2r}\operatorname{csch}^2\left[\frac{\eta}{2}\right], \text{ and } \phi(\eta) = \coth\left[\frac{\eta}{2}\right]. \tag{41}$$

Case 2: $\chi(r) = \frac{24}{25}r^2$.

$$\phi(\eta) = \frac{\tanh[\eta]}{1 \pm 5\operatorname{sech}[\eta]}, \text{ and } \psi(\eta) = \frac{1}{r}\frac{5\operatorname{sech}[\eta]}{5\operatorname{sech}[\eta] \pm 1}. \tag{42}$$

Case 3: $\chi(r) = \frac{5}{9}r^2$.

$$\phi(\eta) = \frac{2}{2\coth[\eta] \pm 3\operatorname{csch}[\eta]}, \text{ and } \psi(\eta) = \frac{1}{r}\frac{3\operatorname{sech}[\eta]}{3\operatorname{sech}[\eta] \pm 2}. \tag{43}$$

Case 4: $\chi(r) = r^2 - 1$.

$$\phi(\eta) = \frac{5\tanh[\eta] + 3}{3\tanh[\eta] + 4r\operatorname{sech}[\eta] + 5}, \text{ and } \psi(\eta) = \frac{4\operatorname{sech}[\eta]}{3\tanh[\eta] + 4r\operatorname{sech}[\eta] + 5}, \tag{44}$$

or

$$\phi(\eta) = \frac{\tanh[\eta]}{r\operatorname{sech}[\eta] + 1}, \text{ and } \psi(\eta) = \frac{\operatorname{sech}[\eta]}{r\operatorname{sech}[\eta] + 1}. \tag{45}$$

Case 5: $\chi(r) = r^2 + 1$.

$$\phi(\eta)=\frac{\coth[\eta]}{r\,\mathrm{csch}[\eta]+1},\ \text{and}\ \ \psi(\eta)=\frac{\mathrm{csch}[\eta]}{r\,\mathrm{csch}[\eta]+1}. \tag{46}$$

4. Novel solitary waves

4.1 *The enhanced direct algebraic scheme*

Balancing U_1'' and ${U_1}^3$ in Eq. (17) causes to

$$U_1(\eta)=\alpha_0+\alpha_1\theta(\eta)+\frac{\beta_1}{\theta(\eta)}. \tag{47}$$

Upon substituting Eqs. (22) and (23) into Eq. (17), a polynomial $\theta(\eta)$ is derived. This polynomial is then manipulated by organizing terms with matching powers and setting the resultant equations to zero, leading to:

$$40\alpha_1\alpha_0^3\beta_1\mho_3+12\alpha_1\alpha_0\beta_1\mho_2+60\alpha_1^2\alpha_0\beta_1^2\mho_3+\alpha_1\tau_1\mho_4+2\alpha_0\left(\alpha_0^4\mho_3+\alpha_0^2\mho_2+\mho_1\right)+\beta_1\tau_3\mho_4+$$

$$\alpha_1k^2\tau_1\tau_2+6\alpha_1k^2\tau_0\tau_3+\beta_1k^2\tau_2\tau_3+6\beta_1k^2\tau_1\tau_4=0,$$

$$10\alpha_1\beta_1^4\mho_3+20\alpha_0^2\beta_1^3\mho_3+4\beta_1\tau_0\mho_4+2\beta_1^3\mho_2+15\beta_1k^2\tau_1^2+40\beta_1k^2\tau_0\tau_2=0,$$

$$20\alpha_0^3\beta_1^2\mho_3+6\alpha_0\beta_1^2\mho_2+40\alpha_1\alpha_0\beta_1^3\mho_3+3\beta_1\tau_1\mho_4+15\beta_1k^2\tau_1\tau_2+30\beta_1k^2\tau_0\tau_3=0,$$

$$20\alpha_1^2\beta_1^3\mho_3+6\alpha_1\beta_1^2\mho_2+60\alpha_0^2\alpha_1\beta_1^2\mho_3+2\beta_1\left(5\alpha_0^4\mho_3+3\alpha_0^2\mho_2+\mho_1\right)+2\beta_1\tau_2\mho_4+2\beta_1k^2\tau_2^2+20\alpha_1^3\beta_1^2\mho_3+$$

$$6\alpha_1^2\beta_1\mho_2+60\alpha_0^2\alpha_1^2\beta_1\mho_3+2\alpha_1\left(5\alpha_0^4\mho_3+3\alpha_0^2\mho_2+\tau_2\left(k^2\tau_2+\mho_4\right)+\mho_1\right)+9\alpha_1k^2\tau_1\tau_3+24\alpha_1k^2\tau_0\tau_4=0,$$

$$40\alpha_0\alpha_1^3\beta_1\mho_3+\alpha_1\left(2\alpha_0\alpha_1\left(10\alpha_0^2\mho_3+3\mho_2\right)+3\tau_3\left(5k^2\tau_2+\mho_4\right)\right)+30\alpha_1k^2\tau_1\tau_4=0,$$

$$10\alpha_1^4\beta_1\mho_3+\alpha_1\left(2\alpha_1^2\left(10\alpha_0^2\mho_3+\mho_2\right)+5k^2\left(3\tau_3^2+8\tau_2\tau_4\right)+4\tau_4\mho_4\right)=0,$$

$$5\alpha_1\left(\alpha_0\alpha_1^3\mho_3+6k^2\tau_3\tau_4\right)=0,$$

$$\alpha_1\left(\alpha_1^4\mho_3+24k^2\tau_4^2\right)=0,$$

$$2\beta_1^5\mho_3+48\beta_1k^2\tau_0^2=0,$$

$$9\beta_1k^2\tau_1\tau_3+24\beta_1k^2\tau_0\tau_4=0,$$

$$10\alpha_0\beta_1^4\mho_3+60\beta_1k^2\tau_0\tau_1=0.$$

The equations are solved, resulting in the following outcomes:
Case 1: $\tau_0 = \tau_1 = \tau_3 = 0$.

$$\alpha_0 = \beta_1 = 0,\ \alpha_1 = \pm\sqrt{\frac{2\tau_4\left(9\tau_2\upsilon_4 + 10\upsilon_1\right)}{\tau_2\upsilon_2}},\ \upsilon_3 = \frac{6\upsilon_2^2\left(\tau_2\upsilon_4 + \upsilon_1\right)}{\left(9\tau_2\upsilon_4 + 10\upsilon_1\right)^2},\ k = \frac{\sqrt{-\tau_2\upsilon_4 - \upsilon_1}}{\tau_2}, \tag{48}$$

$$q(x,\ t) = \pm\sqrt{\frac{-2\left(9\tau_2\upsilon_4 + 10\upsilon_1\right)}{\upsilon_2}}\,\mathrm{sech}\left[\sqrt{\frac{-\left(\tau_2\upsilon_4 + \upsilon_1\right)}{\tau_2}}(x - vt)\right]\ e^{i\left(-\left\{\frac{a_1}{4b_1}\right\}x + \omega t - \sigma^2 t + \sigma W(t) + \theta_0\right)}, \tag{49}$$

$$r(x,\ t) = \Omega\, q(x,\ t), \tag{50}$$

$$q(x,\ t) = \pm\sqrt{\frac{2\left(9\tau_2\upsilon_4 + 10\upsilon_1\right)}{\upsilon_2}}\,\mathrm{csch}\left[\sqrt{\frac{-\left(\tau_2\upsilon_4 + \upsilon_1\right)}{\tau_2}}(x - vt)\right]\ e^{i\left(-\left\{\frac{a_1}{4b_1}\right\}x + \omega t - \sigma^2 t + \sigma W(t) + \theta_0\right)}, \tag{51}$$

$$r(x,\ t) = \Omega\, q(x,\ t). \tag{52}$$

Solutions (49) and (53) are a bright and singular solitons with $\tau_2\left(\tau_2\upsilon_4 + \upsilon_1\right) < 0$.
Case 2: $\tau_0 = \dfrac{\tau_2^2}{4\tau_4},\ \tau_1 = \tau_3 = 0$.
Result 1:

$$\alpha_0 = \beta_1 = 0,\ \alpha_1 = \pm\sqrt{\frac{\tau_4\left(3\tau_2\upsilon_4 + 5\upsilon_1\right)}{\tau_2\upsilon_2}},\ \upsilon_3 = \frac{6\upsilon_2^2\left(\tau_2\upsilon_4 + \upsilon_1\right)}{\left(3\tau_2\upsilon_4 + 5\upsilon_1\right)^2},\ k = \frac{\sqrt{-\left(\tau_2\upsilon_4 + \upsilon_1\right)}}{2\tau_2}, \tag{53}$$

$$q(x,\ t) = \pm\sqrt{\frac{-\left(3\tau_2\upsilon_4 + 5\upsilon_1\right)}{2\upsilon_2}}\,\tanh\left[\sqrt{\frac{\left(\tau_2\upsilon_4 + \upsilon_1\right)}{8\tau_2}}(x - vt)\right]\ e^{i\left(-\left\{\frac{a_1}{4b_1}\right\}x + \omega t - \sigma^2 t + \sigma W(t) + \theta_0\right)}, \tag{54}$$

$$r(x,\ t) = \Omega\, q(x,\ t), \tag{55}$$

$$q(x,\ t) = \pm\sqrt{\frac{-\left(3\tau_2\upsilon_4 + 5\upsilon_1\right)}{2\upsilon_2}}\,\coth\left[\sqrt{\frac{\left(\tau_2\upsilon_4 + \upsilon_1\right)}{8\tau_2}}(x - vt)\right]\ e^{i\left(-\left\{\frac{a_1}{4b_1}\right\}x + \omega t - \sigma^2 t + \sigma W(t) + \theta_0\right)}, \tag{56}$$

$$r(x,\ t) = \Omega\, q(x,\ t). \tag{57}$$

Solutions (54) and (56) are dark and singular solitons with $\tau_2(\tau_2\upsilon_4 + \upsilon_1) > 0$.
Result 2:

$$\alpha_0 = 0,\ \alpha_1 = \pm\sqrt{\frac{\tau_4\left(12\tau_2\upsilon_4 + 5\upsilon_1\right)}{4\tau_2\upsilon_2}},\ \beta_1 = \pm\sqrt{\frac{\tau_2\left(12\tau_2\upsilon_4 + 5\upsilon_1\right)}{16\tau_4\upsilon_2}}, \tag{58}$$

$$\upsilon_3 = \frac{6\upsilon_2^2\left(4\tau_2\upsilon_4 + \upsilon_1\right)}{\left(12\tau_2\upsilon_4 + 5\upsilon_1\right)^2},\ k = \frac{\sqrt{-\left(4\tau_2\upsilon_4 + \upsilon_1\right)}}{8\tau_2},$$

$$q(x,\ t) = \pm\sqrt{\frac{-\left(12\tau_2\upsilon_4 + 5\upsilon_1\right)}{8\upsilon_2}}\left[\tanh\left[\sqrt{-\frac{\left(4\tau_2\upsilon_4 + \upsilon_1\right)}{128\tau_2}}(x - vt)\right] + \coth\left[\sqrt{-\frac{\left(4\tau_2\upsilon_4 + \upsilon_1\right)}{128\tau_2}}(x - vt)\right]\right]$$

$$\times\, e^{i\left(-\left\{\frac{a_1}{4b_1}\right\}x + \omega t - \sigma^2 t + \sigma W(t) + \theta_0\right)}, \tag{59}$$

$$r(x,\ t) = \Omega\ q(x,\ t). \tag{60}$$

Solution (59) is straddled dark-singular soliton with $\tau_2(4\tau_2\upsilon_4 + \upsilon_1) < 0$.

Case 3-1: $\tau_1 = \tau_3 = 0,\ \tau_0 = \dfrac{m^2(1-m^2)\tau_2^2}{(2m^2-1)^2\tau_4}$.

$$\alpha_0 = \beta_1 = 0,\ \alpha_1 = \pm\sqrt{-\frac{2\tau_4\left(3\lambda_1\tau_2\upsilon_4 + 10\lambda_3^2\upsilon_1\right)}{\lambda_2\tau_2\upsilon_2}},\ \upsilon_3 = -\frac{6\lambda_3^2\lambda_2\upsilon_2^2\left(\tau_2\upsilon_4 + \upsilon_1\right)}{\left(3\lambda_1\tau_2\upsilon_4 + 10\lambda_3^2\upsilon_1\right)^2},\ k = \lambda_3\sqrt{\frac{\tau_2\upsilon_4 + \upsilon_1}{\lambda_2\tau_2^2}}, \tag{61}$$

where $\lambda_1 = 16m^4 - 16m^2 + 3,\ \lambda_2 = 8m^4 - 8m^2 - 1,\ \lambda_3 = 2m^2 - 1,$

$$q(x,\ t) = m\sqrt{\frac{2\left(3\lambda_1\tau_2\upsilon_4 + 10\lambda_3^2\upsilon_1\right)}{\lambda_2\upsilon_2(2m^2-1)}}\,\mathrm{cn}\left[\lambda_3\sqrt{\frac{\tau_4\upsilon_4 + \upsilon_1}{(2m^2-1)\lambda_2\tau_2}}(x - vt)\ \middle|\ m\right]\ e^{i\left(-\left\{\frac{a_1}{4b_1}\right\}x + \omega t - \sigma^2 t + \sigma W(t) + \theta_0\right)}, \tag{62}$$

$$r(x,\ t) = \Omega\ q(x,\ t). \tag{63}$$

The result is derived when $m = 1$:

$$q(x,\ t) = \sqrt{\frac{2\left(9\tau_2\upsilon_4 + 10\upsilon_1\right)}{-\upsilon_2}}\ \mathrm{sech}\left[\sqrt{\frac{\tau_4\upsilon_4 + \upsilon_1}{-\tau_2}}(x - vt)\right]\ e^{i\left(-\left\{\frac{a_1}{4b_1}\right\}x + \omega t - \sigma^2 t + \sigma W(t) + \theta_0\right)}, \tag{64}$$

$$r(x,\ t) = \Omega\ q(x,\ t). \tag{65}$$

Solutions (62) and (64) are Jacobi elliptic doubly periodic type and bright soliton solutions.

Result 2:

$$\alpha_0 = 0,\ \beta_1 = \pm m\sqrt{\frac{-2\left(m^2-1\right)\tau_2\left(3\lambda_1\tau_2\upsilon_4+10\lambda_3^2\upsilon_1\right)}{-\lambda_3^2\lambda_2\tau_4\upsilon_2}},\ \upsilon_3 = -\frac{6\lambda_3^2\lambda_2\upsilon_2^2\left(\tau_2\upsilon_4+\upsilon_1\right)}{\left(3\lambda_1\tau_2\upsilon_4+10\lambda_3^2\upsilon_1\right)^2},\ k = \lambda_3\sqrt{\frac{\tau_2\upsilon_4+\upsilon_1}{\lambda_2\tau_2^2}}, \quad (66)$$

where $\lambda_1 = 16m^4-16m^2+3,\ \lambda_2 = 8m^4-8m^2-1,\ \lambda_3 = 2m^2-1,$

$$q(x,\,t) = \sqrt{\frac{-2\left(m^2-1\right)\lambda_3\left(3\lambda_1\tau_2\upsilon_4+10\lambda_3^2\upsilon_1\right)}{\lambda_3^2\lambda_2\upsilon_2}}\ \mathrm{nc}\left[\lambda_3\sqrt{\frac{\tau_4\upsilon_4+\upsilon_1}{(2m^2-1)\lambda_2\tau_2}}(x-vt)\ \middle|\ m\right]$$

$$\times\, e^{i\left(-\left\{\frac{a_1}{4b_1}\right\}x+\omega t-\sigma^2 t+\sigma W(t)+\theta_0\right)}, \quad (67)$$

$$r(x,\,t) = \Omega\, q(x,\,t). \quad (68)$$

Eq. (67) is Jacobi elliptic solution.

Case 3-2: $\tau_1 = \tau_3 = 0,\ \tau_0 = \dfrac{(1-m^2)\tau_2^2}{(2-m^2)^2\tau_4}.$

Result 1:

$$\alpha_0 = 0,\ \alpha_1 = \pm\sqrt{\frac{2\tau_4\left(3\lambda_5\tau_2\upsilon_4+10\lambda_4^2\upsilon_1\right)}{\lambda_6\tau_2\upsilon_2}},\ \upsilon_3 = \frac{6\lambda_4^2\lambda_6\upsilon_2^2\left(\tau_2\upsilon_4+\upsilon_1\right)}{\left(3\lambda_5\tau_2\upsilon_4+10\lambda_4^2\upsilon_1\right)^2},\ k = \lambda_4\sqrt{-\frac{\tau_2\upsilon_4+\upsilon_1}{\lambda_6\tau_2^2}}, \quad (69)$$

where $\lambda_4 = m^2-2,\ \lambda_5 = 3m^4-8m^2+8,\ \lambda_6 = m^4-16m^2+16,$

$$q(x,\,t) = m\sqrt{\frac{2\left(3\lambda_5\tau_2\upsilon_4+10\lambda_4^2\upsilon_1\right)}{\lambda_4\lambda_6\upsilon_2}}\ \mathrm{dn}\left[\sqrt{\frac{\lambda_4(\upsilon_1+\tau_2\upsilon_4)}{\lambda_6\tau_2}}(x-vt)\ \middle|\ m\right]\ e^{i\left(-\left\{\frac{a_1}{4b_1}\right\}x+\omega t-\sigma^2 t+\sigma W(t)+\theta_0\right)}, \quad (70)$$

$$r(x,\,t) = \Omega\, q(x,\,t). \quad (71)$$

For $m = 1$, we get:

$$q(x,\,t) = \sqrt{\frac{2\left(9\tau_2\upsilon_4+10\upsilon_1\right)}{-\upsilon_2}}\ \mathrm{sech}\left[\sqrt{\frac{-(\upsilon_1+\tau_2\upsilon_4)}{\tau_2}}(x-vt)\right]\ e^{i\left(-\left\{\frac{a_1}{4b_1}\right\}x+\omega t-\sigma^2 t+\sigma W(t)+\theta_0\right)}, \quad (72)$$

$$r(x,\,t) = \Omega\, q(x,\,t). \quad (73)$$

Solutions (70) and (72) are Jacobi elliptic doubly periodic type and a bright soliton solutions with $\tau_2\left(\upsilon_1+\tau_2\upsilon_4\right) < 0.$

Result 2:

$$\alpha_0 = 0,\ \beta_1 = \pm\sqrt{-\frac{2\left(m^2-1\right)\tau_2\left(3\lambda_5\tau_2\upsilon_4+10\lambda_4^2\upsilon_1\right)}{\lambda_4^2\lambda_6\tau_4\upsilon_2}},\ \upsilon_3 = \frac{6\lambda_4^2\lambda_6\upsilon_2^2\left(\tau_2\upsilon_4+\upsilon_1\right)}{\left(3\lambda_5\tau_2\upsilon_4+10\lambda_4^2\upsilon_1\right)^2},\ k = \lambda_4\sqrt{-\frac{\tau_2\upsilon_4+\upsilon_1}{\lambda_6\tau_2^2}}, \quad (74)$$

$$q(x,\ t) = \sqrt{-\frac{2\left(m^2-1\right)\left(3\lambda_5\tau_2\upsilon_4+10\lambda_4^2\upsilon_1\right)}{m^2\ \lambda_4\lambda_6\upsilon_2}}\ \mathrm{nd}\left[\sqrt{\frac{\lambda_4(\upsilon_1+\tau_2\upsilon_4)}{\lambda_6\tau_2}}(x-vt)\ \middle|\ m\right]$$

$$\times e^{i\left(-\left\{\frac{a_1}{4b_1}\right\}x+\omega t-\sigma^2 t+\sigma W(t)+\theta_0\right)}, \quad (75)$$

where $\lambda_4 = m^2-2,\ \lambda_5 = 3m^4-8m^2+8,\ \lambda_6 = m^4-16m^2+16,$

$$r(x,\ t) = \Omega\ q(x,\ t). \quad (76)$$

Eq. (75) is Jacobi elliptic solution.

Case 3-3: $\tau_1 = \tau_3 = 0,\ \tau_0 = \dfrac{m^2\tau_2^2}{(m^2+1)^2\tau_4}$.

Result 1:

$$\alpha_0 = 0,\ \alpha_1 = \pm\sqrt{\frac{2\tau_4\left(3\lambda_8\tau_2\upsilon_4+10\lambda_7^2\upsilon_1\right)}{\lambda_9\tau_2\upsilon_2}},\ \upsilon_3 = \frac{6\lambda_7^2\lambda_9\upsilon_2^2\left(\tau_2\upsilon_4+\upsilon_1\right)}{\left(3\lambda_8\tau_2\upsilon_4+10\lambda_7^2\upsilon_1\right)^2},\ k = \lambda_7\sqrt{-\frac{\tau_2\upsilon_4+\upsilon_1}{\lambda_9\tau_2^2}}, \quad (77)$$

where $\lambda_7 = m^2+1,\ \lambda_8 = 3m^4+2m^2+3,\ \lambda_9 = m^4+14m^2+1,$

$$q(x,\ t) = m\sqrt{\frac{-2\left(3\lambda_8\tau_2\upsilon_4+10\lambda_7^2\upsilon_1\right)}{\lambda_9\lambda_7\upsilon_2}}\ \mathrm{sn}\left[\sqrt{-\frac{\lambda_7(\upsilon_1+\tau_2\upsilon_4)}{\lambda_9\tau_2}}(x-vt)\ \middle|\ m\right]\ e^{i\left(-\left\{\frac{a_1}{4b_1}\right\}x+\omega t-\sigma^2 t+\sigma W(t)+\theta_0\right)}, \quad (78)$$

$$r(x,\ t) = \Omega\ q(x,\ t). \quad (79)$$

The result is obtained when $m = 1$:

$$q(x,\ t) = \sqrt{\frac{-\left(3\tau_2\upsilon_4+5\upsilon_1\right)}{2\upsilon_2}}\tanh\left[\sqrt{\frac{\upsilon_1+\tau_2\upsilon_4}{8\tau_2}}(x-vt)\right]\ e^{i\left(-\left\{\frac{a_1}{4b_1}\right\}x+\omega t-\sigma^2 t+\sigma W(t)+\theta_0\right)}, \quad (80)$$

$$r(x,\ t) = \Omega\ q(x,\ t). \quad (81)$$

Solutions (78) and (80) are Jacobi elliptic doubly periodic type and dark soliton solutions.

Result 2:

$$\alpha_0 = 0,\ \beta_1 = \pm m\sqrt{\frac{2\tau_2\left(3\lambda_8\tau_2\upsilon_4 + 10\lambda_7^2\upsilon_1\right)}{\lambda_7^2\lambda_9\tau_4\upsilon_2}},\ \upsilon_3 = \frac{6\lambda_7^2\lambda_9\upsilon_2^2\left(\tau_2\upsilon_4 + \upsilon_1\right)}{\left(3\lambda_8\tau_2\upsilon_4 + 10\lambda_7^2\upsilon_1\right)^2},\ k = \lambda_7\sqrt{-\frac{\tau_2\upsilon_4 + \upsilon_1}{\lambda_9\tau_2^2}}, \tag{82}$$

where $\lambda_7 = m^2 + 1,\ \lambda_8 = 3m^4 + 2m^2 + 3,\ \lambda_9 = m^4 + 14m^2 + 1,$

$$q(x,\ t) = \sqrt{\frac{-2\left(3\lambda_8\tau_2\upsilon_4 + 10\lambda_7^2\upsilon_1\right)}{\lambda_9\lambda_7\upsilon_2}}\ \mathrm{ns}\left[\sqrt{-\frac{\lambda_7(\upsilon_1 + \tau_2\upsilon_4)}{\lambda_9\tau_2}}(x - vt)\ \middle|\ m\right]\ e^{i\left(-\left\{\frac{a_1}{4b_1}\right\}x + \omega t - \sigma^2 t + \sigma W(t) + \theta_0\right)}, \tag{83}$$

$$r(x,\ t) = \Omega\, q(x,\ t). \tag{84}$$

The result is found when $m = 1$:

$$q(x,\ t) = \sqrt{\frac{-\left(3\tau_2\upsilon_4 + 5\upsilon_1\right)}{2\upsilon_2}}\coth\left[\sqrt{\frac{\upsilon_1 + \tau_2\upsilon_4}{8\tau_2}}(x - vt)\right]\ e^{i\left(-\left\{\frac{a_1}{4b_1}\right\}x + \omega t - \sigma^2 t + \sigma W(t) + \theta_0\right)}, \tag{85}$$

$$r(x,\ t) = \Omega\, q(x,\ t). \tag{86}$$

Solutions (83) and (85) are Jacobi elliptic doubly periodic type and singular soliton solutions.
Case 4: $\tau_l = \tau_3 = 0$.
Result 1:

$$\alpha_0 = \beta_1 = 0,\ \alpha_1 = \pm\sqrt{\frac{2\lambda_{10}\tau_4}{\lambda_{11}\upsilon_2}},\ \upsilon_3 = \frac{6\lambda_{11}\lambda_{12}\upsilon_2^2}{\lambda_{10}^2},\ k = \sqrt{-\frac{\lambda_{12}}{\lambda_{11}}}, \tag{87}$$

where $\lambda_{10} = 9\tau_2^2\upsilon_4 + 10\tau_2\upsilon_1 - 12\tau_0\tau_4\upsilon_4,\ \lambda_{11} = \tau_2^2 + 12\tau_0\tau_4,\ \lambda_{12} = \tau_2\upsilon_4 + \upsilon_1,$

$$q(x,\ t) = \pm\sqrt{\frac{2\lambda_{10}}{\lambda_{11}\upsilon_2}}\left[\frac{3\wp'\left(\sqrt{-\frac{\lambda_{12}}{\lambda_{11}}}(x - vt);\ g_2,\ g_3\right)}{\left[6\wp\left(\sqrt{-\frac{\lambda_{12}}{\lambda_{11}}}(x - vt);\ g_2,\ g_3\right) + \tau_2\right]}\right] \times e^{i\left(-\left\{\frac{a_1}{4b_1}\right\}x + \omega t - \sigma^2 t + \sigma W(t) + \theta_0\right)}, \tag{88}$$

$$r(x,\ t) = \Omega\, q(x,\ t). \tag{89}$$

The result is derived when $\tau_0 = 0$:

$$q(x,\ t) = \pm\sqrt{\frac{2\lambda_{10}\tau_2}{\lambda_{12}\upsilon_2}}\left[\mathrm{csch}\left[\sqrt{-\frac{\tau_2\lambda_{12}}{\lambda_{11}}}(x - vt)\right]\right] \times e^{i\left(-\left\{\frac{a_1}{4b_1}\right\}x + \omega t - \sigma^2 t + \sigma W(t) + \theta_0\right)}, \tag{90}$$

$$r(x,\,t)=\Omega\,q(x,\,t), \tag{91}$$

$$q(x,\,t)=\pm\sqrt{\frac{2\lambda_{10}\tau_0\tau_4}{\lambda_{11}\mho_2}}\left[\frac{\left[6\wp\left(\sqrt{-\frac{\lambda_{12}}{\lambda_{11}}}(x-vt);\,g_2,\,g_3\right)+\tau_2\right]}{3\wp'\left(\sqrt{-\frac{\lambda_{12}}{\lambda_{11}}}(x-vt);\,g_2,\,g_3\right)}\right]\times e^{i\left(-\left\{\frac{a_1}{4b_1}\right\}x+\omega t-\sigma^2 t+\sigma W(t)+\theta_0\right)},\ \tau_0>0, \tag{92}$$

$$r(x,\,t)=\Omega\,q(x,\,t). \tag{93}$$

Here $g_2=\dfrac{\tau_2^2}{12}+\tau_0\tau_4$ and $g_3=\dfrac{\tau_2}{216}(36\tau_0\tau_4-\tau_2^2)$. Solution (90) is a singular soliton solution with $\tau_2\lambda_{12}>0$, and $\lambda_{11}<0$.

Result 2:

$$\alpha_0=\alpha_1=0,\ \beta_1=\pm\sqrt{\frac{2\lambda_{10}\tau_0}{\lambda_{11}\mho_2}},\ \mho_3=\frac{6\lambda_{11}\lambda_{12}\mho_2^2}{\lambda_{10}^2},\ k=\sqrt{-\frac{\lambda_{12}}{\lambda_{11}}}, \tag{94}$$

where $\lambda_{10}=9\tau_2^2\mho_4+10\tau_2\mho_1-12\tau_0\tau_4\mho_4,\ \lambda_{11}=\tau_2^2+12\tau_0\tau_4,\ \lambda_{12}=\tau_2\mho_4+\mho_1,$

$$q(x,\,t)=\pm\sqrt{\frac{2\lambda_{10}\tau_0\tau_4}{\lambda_{11}\mho_2}}\left[\frac{\left[6\wp\left(\sqrt{-\frac{\lambda_{12}}{\lambda_{11}}}(x-vt);\,g_2,\,g_3\right)+\tau_2\right]}{3\wp'\left(\sqrt{-\frac{\lambda_{12}}{\lambda_{11}}}(x-vt);\,g_2,\,g_3\right)}\right]\times e^{i\left(-\left\{\frac{a_1}{4b_1}\right\}x+\omega t-\sigma^2 t+\sigma W(t)+\theta_0\right)},\ \tau_4>0, \tag{95}$$

$$r(x,\,t)=\Omega\,q(x,\,t), \tag{96}$$

$$q(x,\,t)=\pm\sqrt{\frac{2\lambda_{10}}{\lambda_{11}\mho_2}}\left[\frac{3\wp'\left(\sqrt{-\frac{\lambda_{12}}{\lambda_{11}}}(x-vt);\,g_2,\,g_3\right)}{\left[6\wp\left(\sqrt{-\frac{\lambda_{12}}{\lambda_{11}}}(x-vt);\,g_2,\,g_3\right)+\tau_2\right]}\right]\times e^{i\left(-\left\{\frac{a_1}{4b_1}\right\}x+\omega t-\sigma^2 t+\sigma W(t)+\theta_0\right)}, \tag{97}$$

$$r(x,\,t)=\Omega\,q(x,\,t), \tag{98}$$

where $g_2=\dfrac{\tau_2^2}{12}+\tau_0\tau_4$ and $g_3=\dfrac{\tau_2}{216}(36\tau_0\tau_4-\tau_2^2)$.

Case 5: $\tau_0=\tau_1=0$.

$$\alpha_0 = \pm\sqrt{\frac{\lambda_{13}}{16\tau_4\upsilon_2}},\ \alpha_1 = \pm\sqrt{\frac{\lambda_{13}\tau_4}{\tau_3^2\upsilon_2}},\ \beta_1 = 0,\ k = \frac{\sqrt{2\lambda_{14}\tau_4}}{\tau_3^2},\ \upsilon_3 = -\frac{48\lambda_{14}\tau_4\upsilon_2^2}{\lambda_{13}^2},\ \tau_2 = \frac{\tau_3^2}{4\tau_4}, \tag{99}$$

$$q(x,\,t) = \pm\sqrt{\frac{\lambda_{13}}{8\tau_4\upsilon_2}}\left[\frac{1}{2} - \frac{\operatorname{sech}^2\left[\frac{\sqrt{\lambda_{14}}}{2\sqrt{2}\tau_3}(x-vt)\right]}{\pm\left[\tanh\left[\frac{\sqrt{\lambda_{14}}}{2\sqrt{2}\tau_3}(x-vt)\right]+1\right]}\right] e^{i\left(-\left\{\frac{a_1}{4b_1}\right\}x+\omega t-\sigma^2 t+\sigma W(t)+\theta_0\right)},\ \tau_4 > 0, \tag{100}$$

$$r(x,\,t) = \Omega\, q(x,\,t), \tag{101}$$

$$q(x,\,t) = \pm\sqrt{\frac{\lambda_{13}}{8\tau_4\upsilon_2}}\left[\frac{1}{2} + \frac{\operatorname{csch}^2\left[\frac{\sqrt{\lambda_{14}}}{2\sqrt{2}\tau_3}(x-vt)\right]}{\pm\left[\coth\left[\frac{\sqrt{\lambda_{14}}}{2\sqrt{2}\tau_3}(x-vt)\right]+1\right]}\right] e^{i\left(-\left\{\frac{a_1}{4b_1}\right\}x+\omega t-\sigma^2 t+\sigma W(t)+\theta_0\right)},\ \tau_4 > 0, \tag{102}$$

$$r(x,\,t) = \Omega\, q(x,\,t), \tag{103}$$

$$q(x,\,t) = \pm\sqrt{\frac{\lambda_{13}}{16\tau_4\upsilon_2}}\left[1 - \frac{\operatorname{sech}^2\left[\frac{\sqrt{\lambda_{14}}}{2\sqrt{2}\tau_3}(x-vt)\right]}{\left[1-\frac{1}{4}\left(1+\tanh\left[\frac{\sqrt{\lambda_{14}}}{2\sqrt{2}\tau_3}(x-vt)\right]\right)^2\right]}\right] e^{i\left(-\left\{\frac{a_1}{4b_1}\right\}x+\omega t-\sigma^2 t+\sigma W(t)+\theta_0\right)}, \tag{104}$$

$$r(x,\,t) = \Omega\, q(x,\,t), \tag{105}$$

$$q(x,\,t) = \pm\sqrt{\frac{\lambda_{13}}{16\tau_4\upsilon_2}}\left[1 + \frac{\operatorname{csch}^2\left[\frac{\sqrt{\lambda_{14}}}{2\sqrt{2}\tau_3}(x-vt)\right]}{\left[1-\frac{1}{4}\left(1+\coth\left[\frac{\sqrt{\lambda_{14}}}{2\sqrt{2}\tau_3}(x-vt)\right]\right)^2\right]}\right] e^{i\left(-\left\{\frac{a_1}{4b_1}\right\}x+\omega t-\sigma^2 t+\sigma W(t)+\theta_0\right)}, \tag{106}$$

$$r(x,\,t) = \Omega\, q(x,\,t). \tag{107}$$

Eqs. (102) and (106) are singlar-singular solitons, while Eqs. (100) and (104) are bright-dark solitons.

4.2 *The projective Riccati equations algorithm*

Balancing ${U_1}''$ and ${U_1}^3$ in Eq. (17) yields

$$Q_1(\eta) = \alpha_0 + \alpha_1\psi(\eta) + \beta_1\phi(\eta). \tag{108}$$

Here $\alpha_0,\ \alpha_1$, and β_1 are constants, where $\alpha_1 \neq 0$ or $\beta_1 \neq 0$. Inserting Eq. (108) together with Eq. (38) and Eq. (39) into Eq. (17) results in:

$$30\alpha_1\alpha_0^2\beta_1^2\upsilon_3 + 3\alpha_1\beta_1^2\upsilon_2 + 5\alpha_1\beta_1^4\upsilon_3 + 5\alpha_1\alpha_0^4\upsilon_3 + 3\alpha_1\alpha_0^2\upsilon_2 + \alpha_1\upsilon_1 + \alpha_1\upsilon_4 + \alpha_1k^2 - 20\alpha_0^3\beta_1^2r\upsilon_3$$

$$- 6\alpha_0\beta_1^2r\upsilon_2 - 20\alpha_0\beta_1^4r\upsilon_3 = 0,$$

$$30\alpha_0\alpha_1^2\beta_1^2\upsilon_3 + 3\alpha_0\alpha_1^2\upsilon_2 + 10\alpha_0^3\alpha_1^2\upsilon_3 - 15\alpha_1k^2r + 20\alpha_0\beta_1^4r^2\upsilon_3 - 20\alpha_1\beta_1^4r\upsilon_3 - 6\alpha_1\beta_1^2r\upsilon_2$$

$$- 60\alpha_0^2\alpha_1\beta_1^2r\upsilon_3 - 3\alpha_1r\upsilon_4 + 10\alpha_0\beta_1^4\upsilon_3R(r) + 3\alpha_0\beta_1^2\upsilon_2R(r) + 10\alpha_0^3\beta_1^2\upsilon_3R(r) = 0,$$

$$10\alpha_1^3\beta_1^2\upsilon_3 + \alpha_1^3\upsilon_2 + 10\alpha_0^2\alpha_1^3\upsilon_3 + 30\alpha_1k^2r^2 + 20\alpha_1k^2R(r) + 20\alpha_1\beta_1^4r^2\upsilon_3 - 60\alpha_0\alpha_1^2\beta_1^2r\upsilon_3$$

$$- 20\alpha_0\beta_1^4r\upsilon_3R(r) + 10\alpha_1\beta_1^4\upsilon_3R(r) + 3\alpha_1\beta_1^2\upsilon_2R(r) + 30\alpha_0^2\alpha_1\beta_1^2\upsilon_3R(r) + 2\alpha_1\upsilon_4R(r) = 0,$$

$$5\alpha_0\alpha_1^4\upsilon_3 - 60\alpha_1k^2rR(r) - 20\alpha_1^3\beta_1^2r\upsilon_3 + 30\alpha_0\alpha_1^2\beta_1^2\upsilon_3R(r) - 20\alpha_1\beta_1^4r\upsilon_3R(r) + 5\alpha_0\beta_1^4\upsilon_3R(r)^2 = 0,$$

$$10\alpha_1^2\beta_1^3\upsilon_3 + 3\alpha_1^2\beta_1\upsilon_2 + 30\alpha_0^2\alpha_1^2\beta_1\upsilon_3 + 6\beta_1k^2r^2 + 8\beta_1k^2R(r) + 4\beta_1^5r^2\upsilon_3 - 40\alpha_0\alpha_1\beta_1^3r\upsilon_3$$

$$+ 10\alpha_0^2\beta_1^3\upsilon_3R(r) + 2\beta_1^5\upsilon_3R(r) + \beta_1^3\upsilon_2R(r) + 2\beta_1\upsilon_4R(r) = 0,$$

$$20\alpha_0\alpha_1^3\beta_1\upsilon_3 - 36\beta_1k^2rR(r) - 20\alpha_1^2\beta_1^3r\upsilon_3 + 20\alpha_0\alpha_1\beta_1^3\upsilon_3R(r) - 4\beta_1^5r\upsilon_3R(r) = 0,$$

$$5\alpha_1^4\beta_1\upsilon_3 + 24\beta_1k^2R(r)^2 + 10\alpha_1^2\beta_1^3\upsilon_3R(r) + \beta_1^5\upsilon_3R(r)^2 = 0,$$

$$20\alpha_0\alpha_1\beta_1^3\upsilon_3 + 6\alpha_0\alpha_1\beta_1\upsilon_2 + 20\alpha_0^3\alpha_1\beta_1\upsilon_3 - \beta_1k^2r - 20\alpha_0^2\beta_1^3r\upsilon_3 - 4\beta_1^5r\upsilon_3 - 2\beta_1^3r\upsilon_2 - \beta_1r\upsilon_4 = 0,$$

$$10\alpha_0^2\beta_1^3\upsilon_3 + 3\alpha_0^2\beta_1\upsilon_2 + 5\alpha_0^4\beta_1\upsilon_3 + \beta_1^5\upsilon_3 + \beta_1^3\upsilon_2 + \beta_1\upsilon_1 = 0,$$

$$10\alpha_0^3\beta_1^2\upsilon_3 + 3\alpha_0\beta_1^2\upsilon_2 + 5\alpha_0\beta_1^4\upsilon_3 + \alpha_0^5\upsilon_3 + \alpha_0^3\upsilon_2 + \alpha_0\upsilon_1 = 0,$$

$$\alpha_1^5\upsilon_3 + 24\alpha_1k^2R(r)^2 + 10\alpha_1^3\beta_1^2\upsilon_3R(r) + 5\alpha_1\beta_1^4\upsilon_3R(r)^2 = 0.$$

The equations are solved, resulting in the following outcomes:
Case 1: $\chi(r) = 0$.

$$\alpha_0 = \alpha_1 = 0,\ \beta_1 = \pm\sqrt{\frac{3\upsilon_4 - 10\upsilon_1}{4\upsilon_2}},\ \upsilon_3 = \frac{12\upsilon_2^2(2\upsilon_1 - \upsilon_4)}{(10\upsilon_1 - 3\upsilon_4)^2},\ k = \sqrt{\frac{(\upsilon_4 - 2\upsilon_1)}{2}}, \tag{109}$$

$$q(x,\,t) = \pm\sqrt{\frac{3\mho_4 - 10\mho_1}{4\mho_2}}\tanh\left[\sqrt{\frac{-2\mho_1+\mho_4}{8}}(x-vt)\right]\, e^{i\left(-\left\{\frac{a_1}{4b_1}\right\}x+\omega t-\sigma^2 t+\sigma W(t)+\theta_0\right)}, \tag{110}$$

$$r(x,\,t) = \Omega\, q(x,\,t), \tag{111}$$

$$q(x,\,t) = \pm\sqrt{\frac{3\mho_4 - 10\mho_1}{4\mho_2}}\coth\left[\sqrt{\frac{-2\mho_1+\mho_4}{8}}(x-vt)\right]\, e^{i\left(-\left\{\frac{a_1}{4b_1}\right\}x+\omega t-\sigma^2 t+\sigma W(t)+\theta_0\right)}, \tag{112}$$

$$r(x,\,t) = \Omega\, q(x,\,t). \tag{113}$$

Solutions (110) and (112) are dark and singular solitons.

Case 2: $\chi(r) = \dfrac{24r^2}{25}$.

$$\alpha_0 = 0,\ \alpha_1 = \pm\sqrt{-\frac{6r^2\,(10\mho_1 - 3\mho_4)}{25\mho_2}},\ \beta_1 = \pm\sqrt{\frac{3\mho_4 - 10\mho_1}{4\mho_2}},\ \mho_3 = \frac{12\mho_2^2\,(2\mho_1 - \mho_4)}{(10\mho_1 - 3\mho_4)^2},\ k = \sqrt{\frac{(\mho_4 - 2\mho_1)}{2}}, \tag{114}$$

$$q(x,\,t) = \pm\sqrt{\frac{(3\mho_4 - 10\mho_1)}{\mho_2}}\left[\frac{\sqrt{6}\,\mathrm{sech}\left[\sqrt{\frac{(\mho_4 - 2\mho_1)}{2}}(x-vt)\right]}{5\,\mathrm{sech}\left[\sqrt{\frac{(\mho_4 - 2\mho_1)}{2}}(x-vt)\right]\pm 1} + \frac{1}{2}\frac{\tanh\left[\sqrt{\frac{(\mho_4 - 2\mho_1)}{2}}(x-vt)\right]}{1\pm 5\,\mathrm{sech}\left[\sqrt{\frac{(\mho_4 - 2\mho_1)}{2}}(x-vt)\right]}\right] \tag{115}$$

$$\times\, e^{i\left(-\left\{\frac{a_1}{4b_1}\right\}x+\omega t-\sigma^2 t+\sigma W(t)+\theta_0\right)}, \tag{116}$$

$$r(x,\,t) = \Omega\, q(x,\,t). \tag{117}$$

Solution (115) is a straddled bright-dark solitons.

Case 3: $\chi(r) = \dfrac{5r^2}{9}$.

$$\alpha_0 = 0,\ \alpha_1 = \pm\sqrt{\frac{5r^2\left(3\mho_4 - 10\mho_1\right)}{36\mho_2}},\ \beta_1 = \pm\sqrt{\frac{3\mho_4 - 10\mho_1}{8\mho_2}},\ \mho_3 = \frac{12\mho_2^2\left(2\mho_1 - \mho_4\right)}{\left(10\mho_1 - 3\mho_4\right)^2},\ k = \sqrt{\frac{\left(\mho_4 - 2\mho_1\right)}{2}}, \tag{118}$$

$$q(x,\ t) = \pm\sqrt{\frac{3\mho_4 - 10\mho_1}{2\mho_2}}\left[\frac{\operatorname{sech}\left[\sqrt{\frac{\left(\mho_4 - 2\mho_1\right)}{2}}(x - vt)\right]}{\sqrt{2}\left(3\operatorname{sech}\left[\sqrt{\frac{\left(\mho_4 - 2\mho_1\right)}{2}}(x - vt)\right] \pm 2\right)}\right.$$

$$\left. + \frac{1}{2\coth\left[\sqrt{\frac{\left(\mho_4 - 2\mho_1\right)}{2}}(x - vt)\right] \pm 3\operatorname{csch}\left[\sqrt{\frac{\left(\mho_4 - 2\mho_1\right)}{2}}(x - vt)\right]}\right] \times e^{i\left(-\left\{\frac{a_1}{4b_1}\right\}x + \omega t - \sigma^2 t + \sigma W(t) + \theta_0\right)}, \tag{119}$$

$$r(x,\ t) = \Omega\, q(x,\ t). \tag{120}$$

Solution (119) is a straddled bright-singular soliton.
Case 4: $\chi(r) = r^2 - 1$.

$$\alpha_0 = 0,\ \alpha_1 = \pm\sqrt{\frac{\left(r^2 - 1\right)\left(3\mho_4 - 10\mho_1\right)}{4\mho_2}},\ \beta_1 = \pm\sqrt{\frac{3\mho_4 - 10\mho_1}{4\mho_2}},$$

$$\mho_3 = \frac{12\mho_2^2\left(2\mho_1 - \mho_4\right)}{\left(10\mho_1 - 3\mho_4\right)^2},\ k = \sqrt{\frac{\left(\mho_4 - 2\mho_1\right)}{2}}, \tag{121}$$

$$q(x,\ t) = \pm\sqrt{\frac{3\mho_4 - 10\mho_1}{4\mho_2}}\left[\left[\frac{2\sqrt{r^2 - 1}\operatorname{sech}\left[\sqrt{\frac{\left(\mho_4 - 2\mho_1\right)}{2}}(x - vt)\right]}{3\tanh\left[\sqrt{\frac{\left(\mho_4 - 2\mho_1\right)}{2}}(x - vt)\right] + 4r\operatorname{sech}\left[\sqrt{\frac{\left(\mho_4 - 2\mho_1\right)}{2}}(x - vt)\right] + 5}\right]\right.$$

$$\left. + \left[\frac{5\tanh\left[\sqrt{\frac{\left(\mho_4 - 2\mho_1\right)}{2}}(x - vt)\right] + 3}{3\tanh\left[\sqrt{\frac{\left(\mho_4 - 2\mho_1\right)}{2}}(x - vt)\right] + 4r\operatorname{sech}\left[\sqrt{\frac{\left(\mho_4 - 2\mho_1\right)}{2}}(x - vt)\right] + 5}\right]\right]$$

$$\times e^{i\left(-\left\{\frac{a_1}{4b_1}\right\}x + \omega t - \sigma^2 t + \sigma W(t) + \theta_0\right)}, \tag{122}$$

$$r(x,\,t) = \Omega\, q(x,\,t), \tag{123}$$

$$q(x,\,t) = \pm\sqrt{\frac{3\mho_4 - 10\mho_1}{4\mho_2}}\left[\frac{\sqrt{r^2-1}\,\mathrm{sech}\left[\sqrt{\frac{(\mho_4-2\mho_1)}{2}}(x-vt)\right]}{r\,\mathrm{sech}\left[\sqrt{\frac{(\mho_4-2\mho_1)}{2}}(x-vt)\right]+1} + \frac{\tanh\left[\sqrt{\frac{(\mho_4-2\mho_1)}{2}}(x-vt)\right]}{r\,\mathrm{sech}\left[\sqrt{\frac{(\mho_4-2\mho_1)}{2}}(x-vt)\right]+1}\right] \tag{124}$$

$$\times e^{i\left(-\left\{\frac{a_1}{4b_1}\right\}x+\omega t-\sigma^2 t+\sigma W(t)+\theta_0\right)}, \tag{125}$$

$$r(x,\,t) = \Omega\, q(x,\,t). \tag{126}$$

Solutions (122) and (124) are straddled bright-dark solitons.
Case 5: $\chi(r) = r^2 + 1$.

$$\alpha_0 = 0,\ \alpha_1 = \pm\sqrt{\frac{(r^2+1)\,(3\mho_4 - 10\mho_1)}{8\mho_2}},\ \beta_1 = \pm\sqrt{\frac{3\mho_4 - 10\mho_1}{8\mho_2}},$$

$$\mho_3 = \frac{12\mho_2^2\,(2\mho_1 - \mho_4)}{(10\mho_1 - 3\mho_4)^2},\ k = \sqrt{\frac{(\mho_4 - 2\mho_1)}{2}}, \tag{127}$$

$$q(x,\,t) = \pm\sqrt{\frac{3\mho_4 - 10\mho_1}{8\mho_2}}\left[\frac{\sqrt{(1+r^2)}\,\mathrm{csch}\left[\sqrt{\frac{(\mho_4-2\mho_1)}{2}}(x-vt)\right]}{r\,\mathrm{csch}\left[\sqrt{\frac{(\mho_4-2\mho_1)}{2}}(x-vt)\right]+1} + \frac{\coth\left[\sqrt{\frac{(\mho_4-2\mho_1)}{2}}(x-vt)\right]}{r\,\mathrm{csch}\left[\sqrt{\frac{(\mho_4-2\mho_1)}{2}}(x-vt)\right]+1}\right] \tag{128}$$

$$\times\, e^{i\left(-\left\{\frac{a_1}{4b_1}\right\}x+\omega t-\sigma^2 t+\sigma W(t)+\theta_0\right)}, \tag{129}$$

$$r(x,\,t) = \Omega\, q(x,\,t). \tag{130}$$

A singular-singular soliton is identified in solution (128).

5. Results and discussion

This section provides an in-depth examination of the findings presented in Figures 1-24, focusing on the progression and characteristics of various soliton solutions described by complex-valued functions. The simulations are based on a set of specific parameter values: $\tau_2 = 1.9$, $\theta_0 = 1.1$, $a_1 = 4$, $b_1 = 1$, $\omega = 1.4$, $k = 1.8$, $\alpha_1 = 2.3$, $\Omega = 2.4$, $\beta_1 = 3.1$, $f_1 = 3.9$, and $g_1 = 3.2$. These parameters shape the evolution of distinct soliton types, including singular-singular, bright-

dark, singular, dark, and bright solitons. The impact of multiplicative white noise (σ) is assessed by setting its value to 0, 2, 3, and 4, allowing a detailed analysis of noise influence on soliton stability and structural integrity.

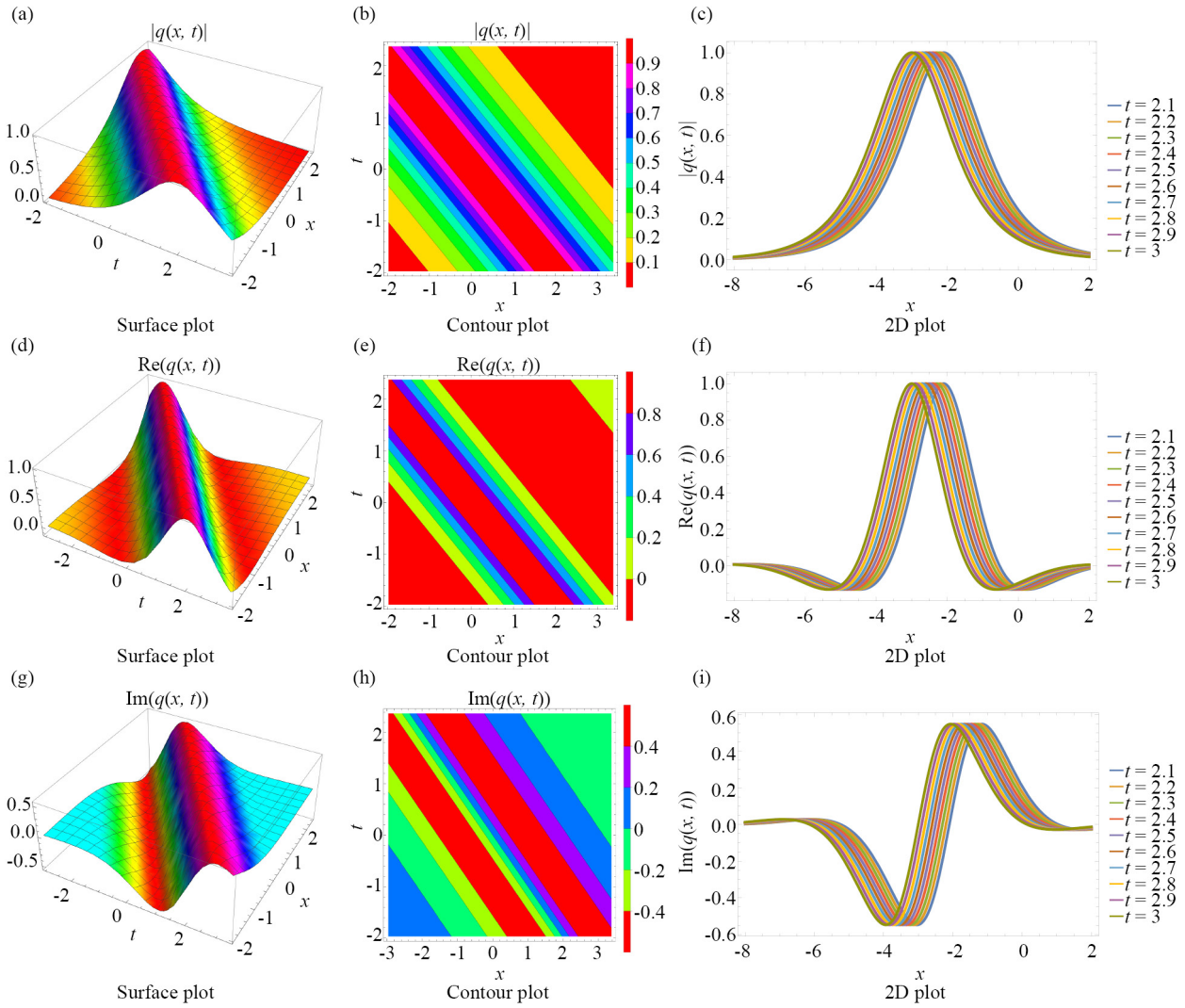

Figure 1. A bright soliton given $\sigma = 0$

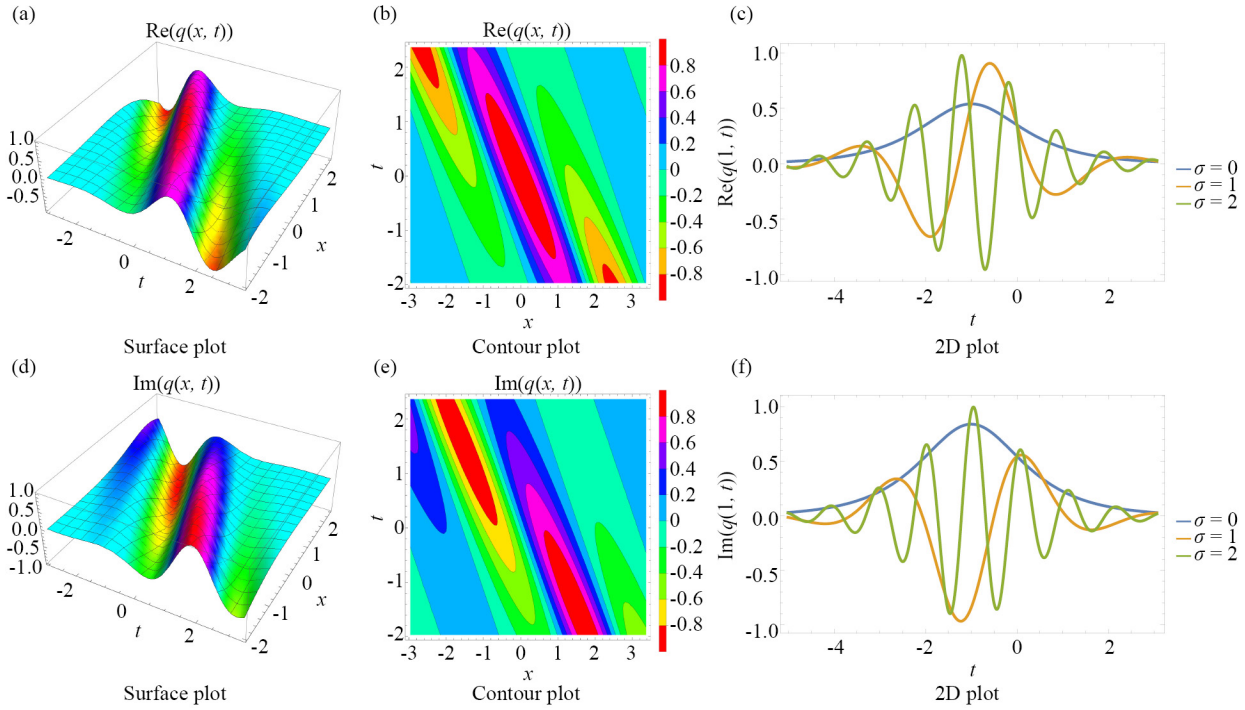

Figure 2. A bright soliton given $\sigma = 2$

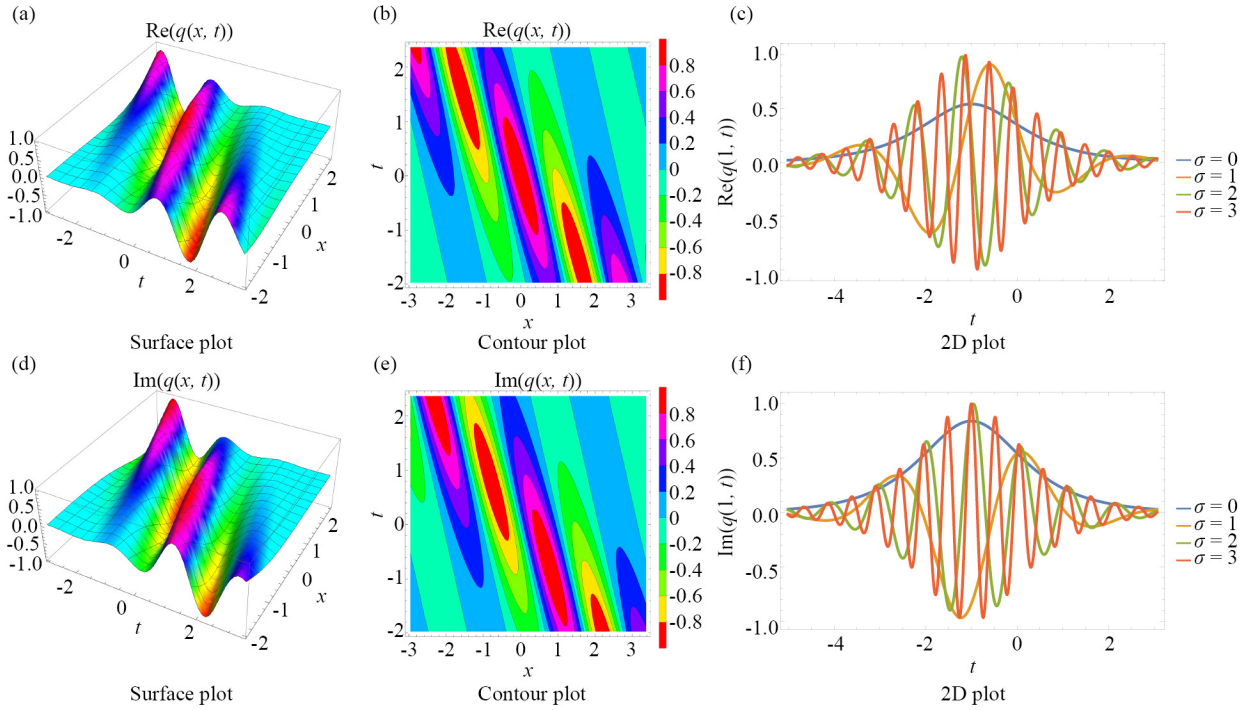

Figure 3. A bright soliton given $\sigma = 3$

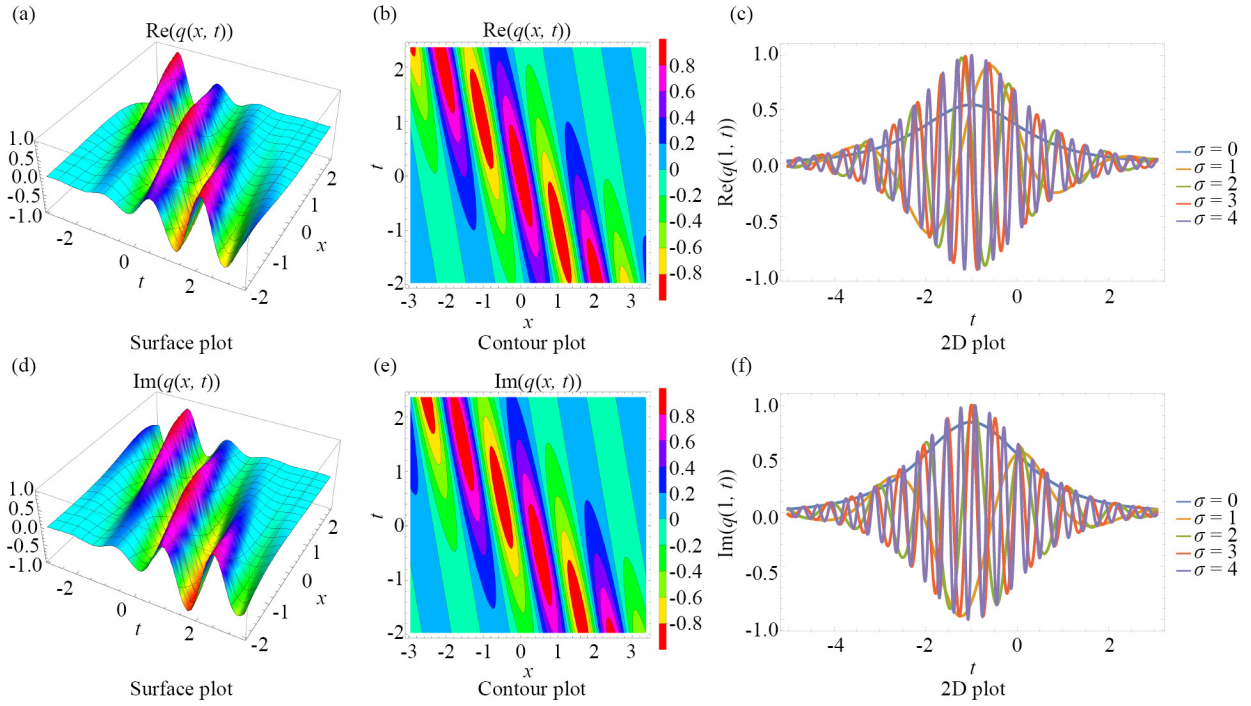

Figure 4. A bright soliton given $\sigma = 4$

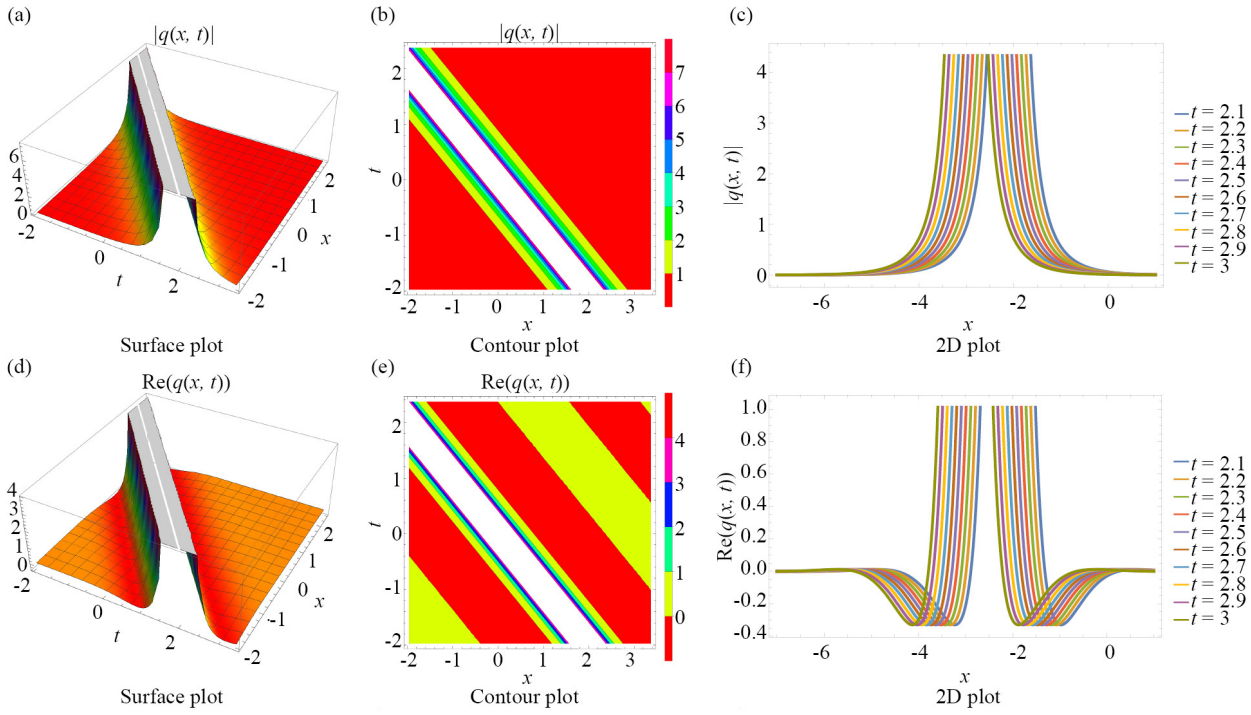

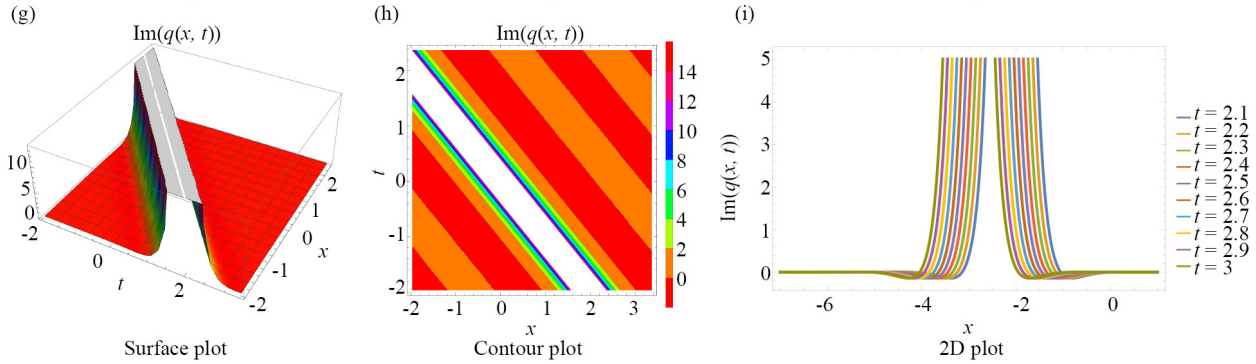

Figure 5. A singular soliton given $\sigma = 0$

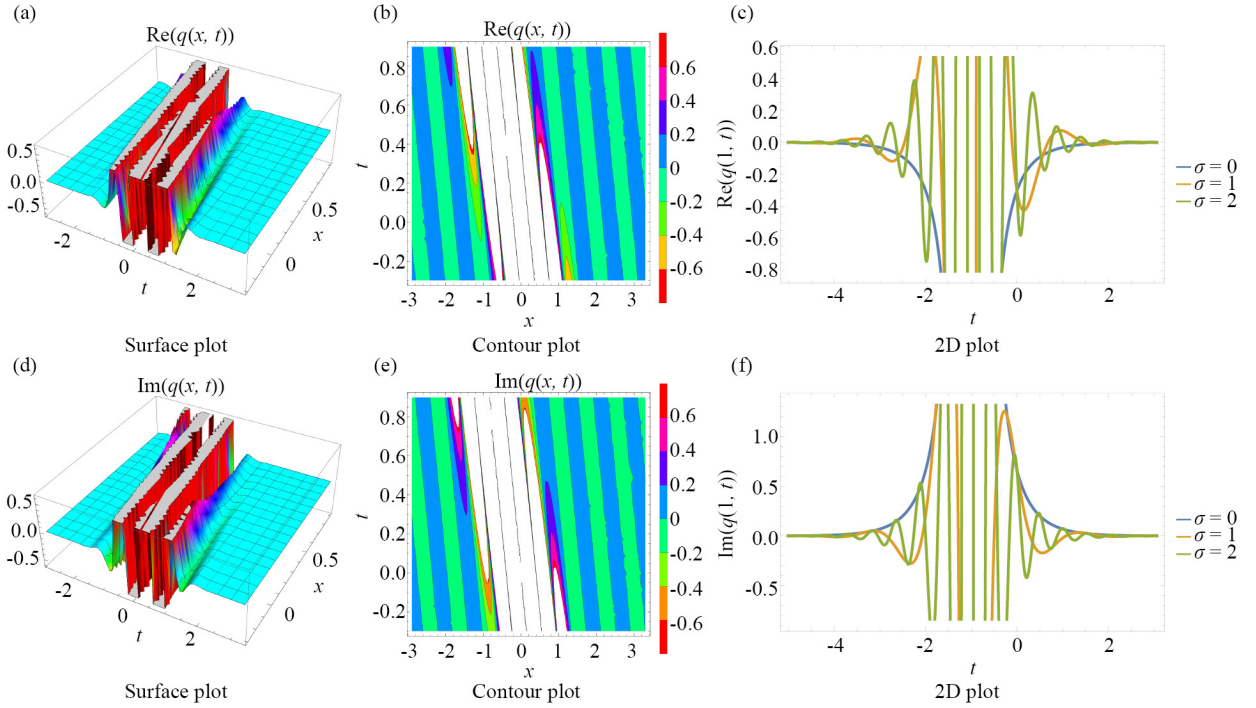

Figure 6. A singular soliton given $\sigma = 2$

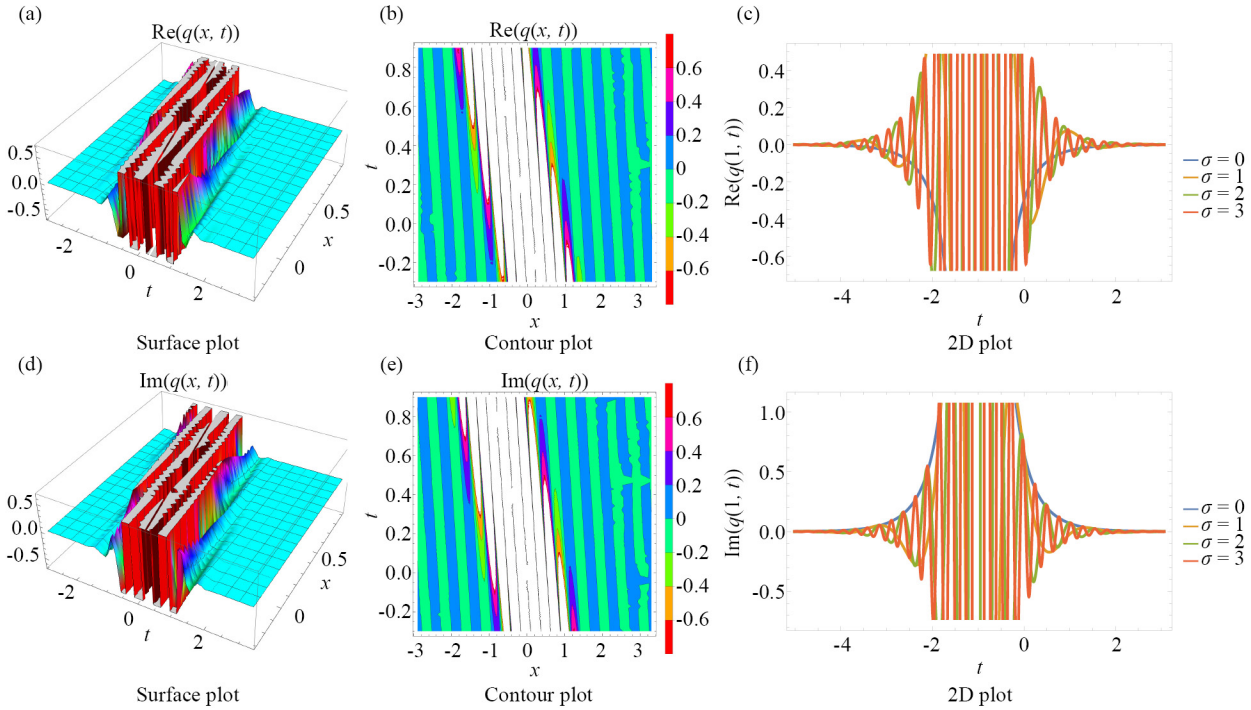

Figure 7. A singular soliton given $\sigma = 3$

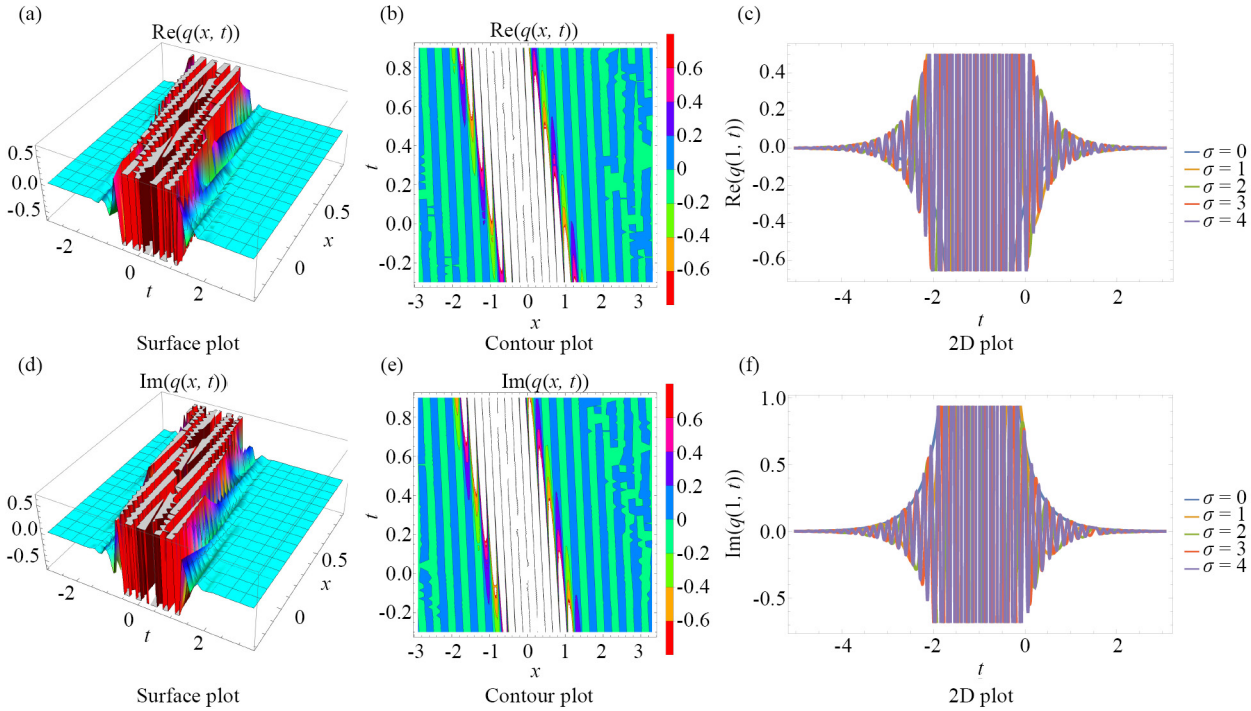

Figure 8. A singular soliton given $\sigma = 4$

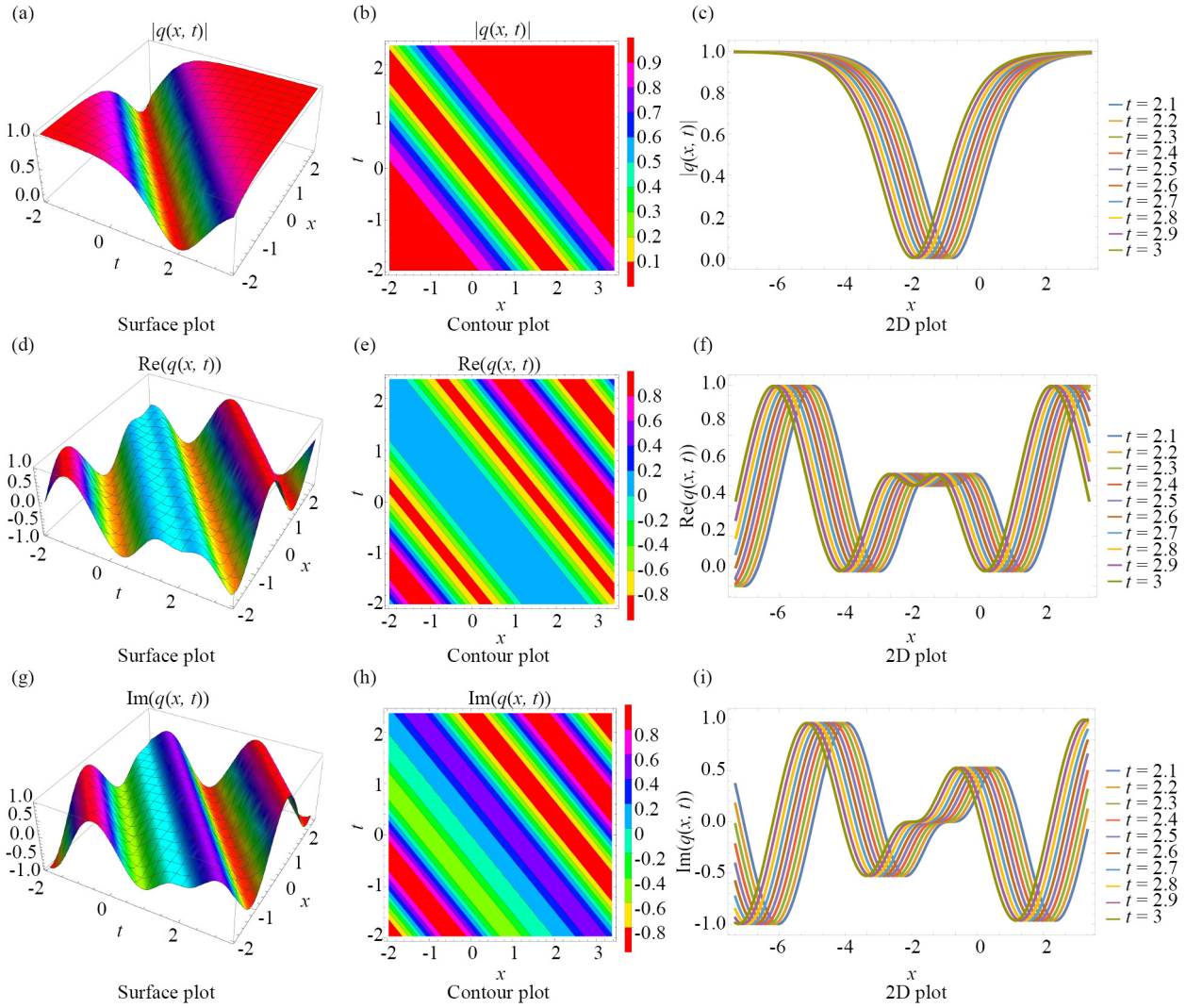

Figure 9. A dark soliton given $\sigma = 0$

Figures 1-4 provide insight into the bright soliton solution, described by solution (49). Figure 1 serves as a baseline, visualizing the bright soliton without the influence of multiplicative white noise through a range of representations: 2D, contour, and surface plots of the modulus, real part, and imaginary part. Specifically, Figures 1a, 1b, and 1c illustrate the modulus; Figures 1d, 1e, and 1f show the real part; and Figures 1g, 1h, and 1i display the imaginary part. Figures 2-4 then explore the effect of varying levels of multiplicative white noise with σ values set at 2, 3, and 4, respectively. Each figure includes comprehensive 2D, contour, and surface plots for the real and imaginary parts, demonstrating that as the σ value rises, the bright soliton structure becomes progressively distorted. This distortion highlights the noise's destabilizing effect, as evidenced by increasingly irregular patterns within the contour and 2D visualizations. Figures 5-8 shift focus to the singular soliton solution, represented by solution (51). Figure 5 depicts the singular soliton without any added noise, utilizing modulus, real part, and imaginary part visualizations similar to those used for the bright soliton. The distinctive singular nature of this soliton is evident through pronounced peaks and valleys within the surface plots. Figures 6-8 introduce varying levels of multiplicative white noise, set at $\sigma = 2,\ 3,\ 4$. This addition of noise induces significant alterations in the soliton's properties, producing disruptions and irregularities within the real and imaginary components. As σ increases, these irregularities become more apparent, emphasizing the heightened sensitivity of singular soliton solutions to external perturbations. Figures 9-12 illustrate the dark soliton solution $q(x,\ t)$, derived from solution (54).

Figure 9, devoid of noise, showcases the characteristic dip in amplitude, typical of dark solitons, across 2D, contour, and surface plots of the real and imaginary parts. The dip is highly localized, underscoring the dark soliton's unique reduction in amplitude. Figures 10-12 add the influence of multiplicative white noise at σ levels of 2, 3, and 4. As noise is introduced, fluctuations emerge in the soliton's profile, especially evident in the contour and 2D representations. These visualizations indicate that the structure of the dark soliton is increasingly disrupted with higher noise levels, revealing its relative vulnerability to noise interference. Figures 13-16 continue with another singular soliton solution $q(x,\ t)$, represented by solution (56). Like Figure 5, Figure 13, without noise, provides the modulus, imaginary, and real parts across various visual formats, showcasing the soliton's singular characteristics with sharp, prominent peaks in the surface plots. Figures 14-16 depict the effects of adding multiplicative white noise at values of $\sigma = 2,\ 3,\ 4$. As the noise level grows, the singular soliton's structure displays greater instability, similar to the trends observed for the singular soliton in Figures 6-8. Noise disruptions produce erratic patterns within the contour and 2D plots, which become more severe as σ increases. Figures 17-20 delve into the bright-dark soliton solution, depicted by solution (100). Figure 17 provides a baseline view, without noise, where the mixed features of bright and dark solitons are evident across the modulus, imaginary, and real parts. Figures 18-20 analyze the impact of multiplicative white noise at σ values of 2, 3, and 4. Here, the combined soliton structures undergo notable disturbance as noise escalates, leading to increasingly complex and irregular patterns within the real and imaginary components. With higher σ values, both the bright and dark components of the soliton become visibly distorted, illustrating the significant effect of noise on this mixed soliton type. Figures 21-24 cover the singular-singular soliton solution $q(x,\ t)$, described by solution (102). Figure 21, without noise, emphasizes the singular nature of both solitons through 2D, contour, and surface plots. Figures 22-24 reveal the role of multiplicative white noise at σ values of 2, 3, and 4. Consistent with previous observations for singular solitons, the introduction of noise induces substantial perturbations, leading to highly irregular patterns in the soliton profile. The singular-singular soliton shows a pronounced sensitivity to noise, with increasing σ levels leading to greater structural instability and erratic behavior.

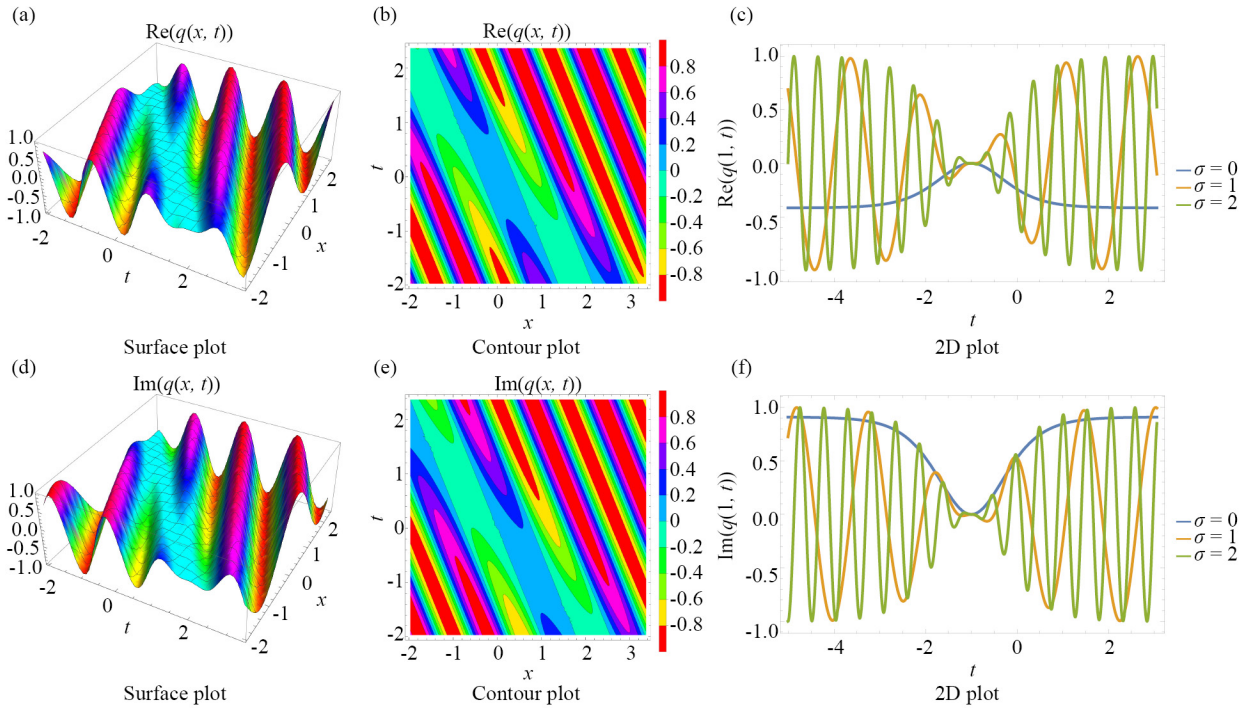

Figure 10. A dark soliton given $\sigma = 2$

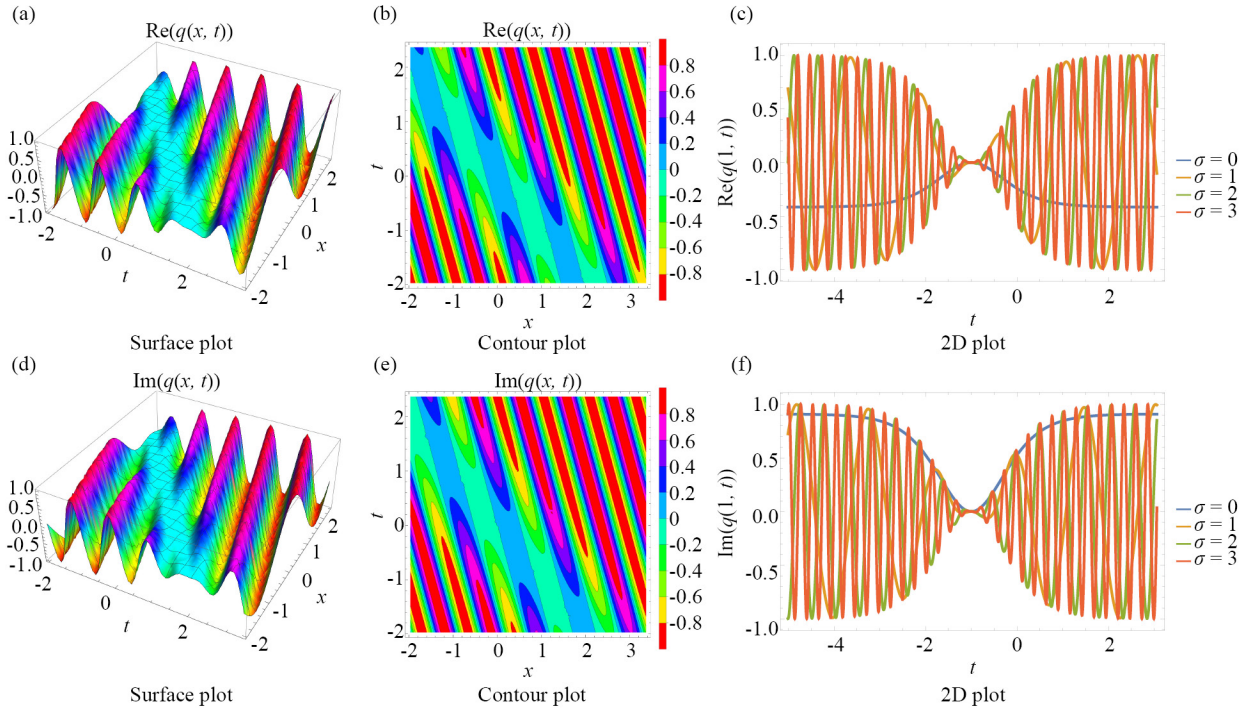

Figure 11. A dark soliton given $\sigma = 3$

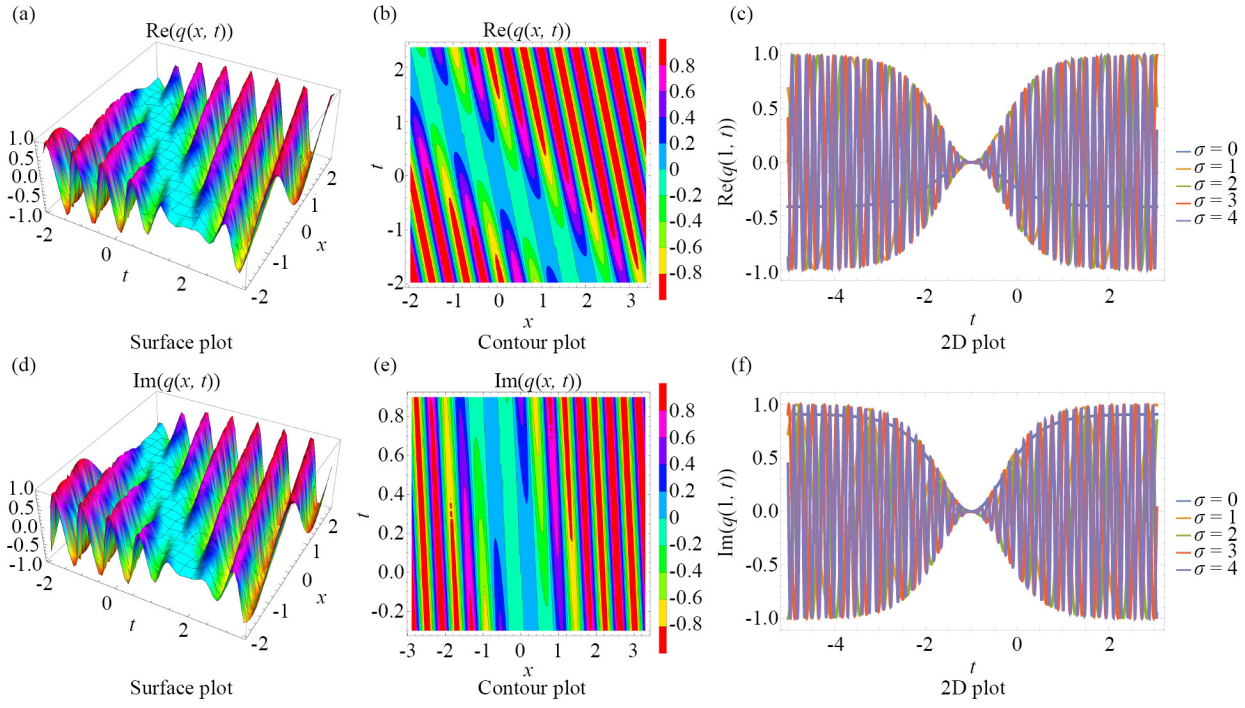

Figure 12. A dark soliton given $\sigma = 4$

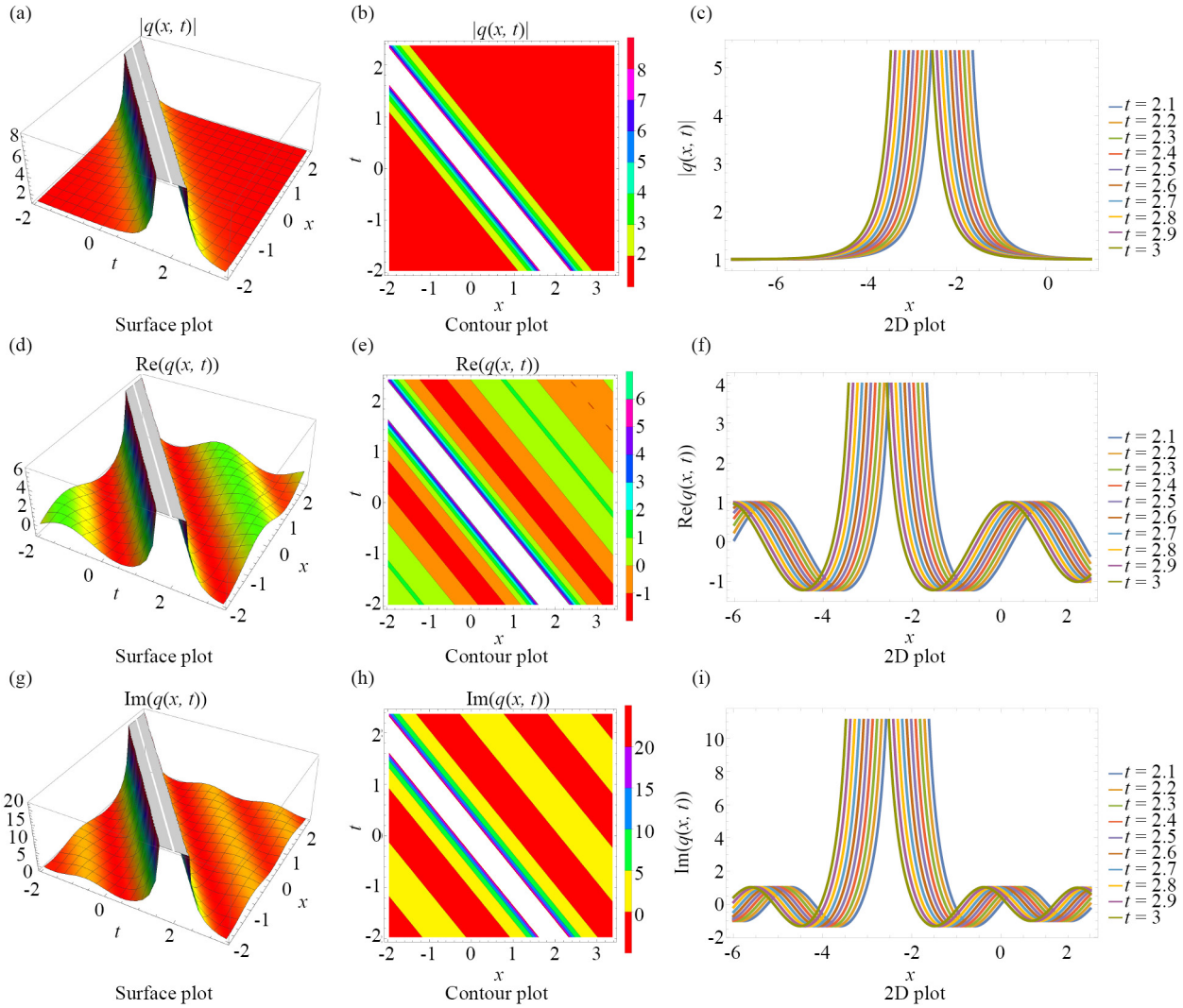

Figure 13. A singular soliton given $\sigma = 0$

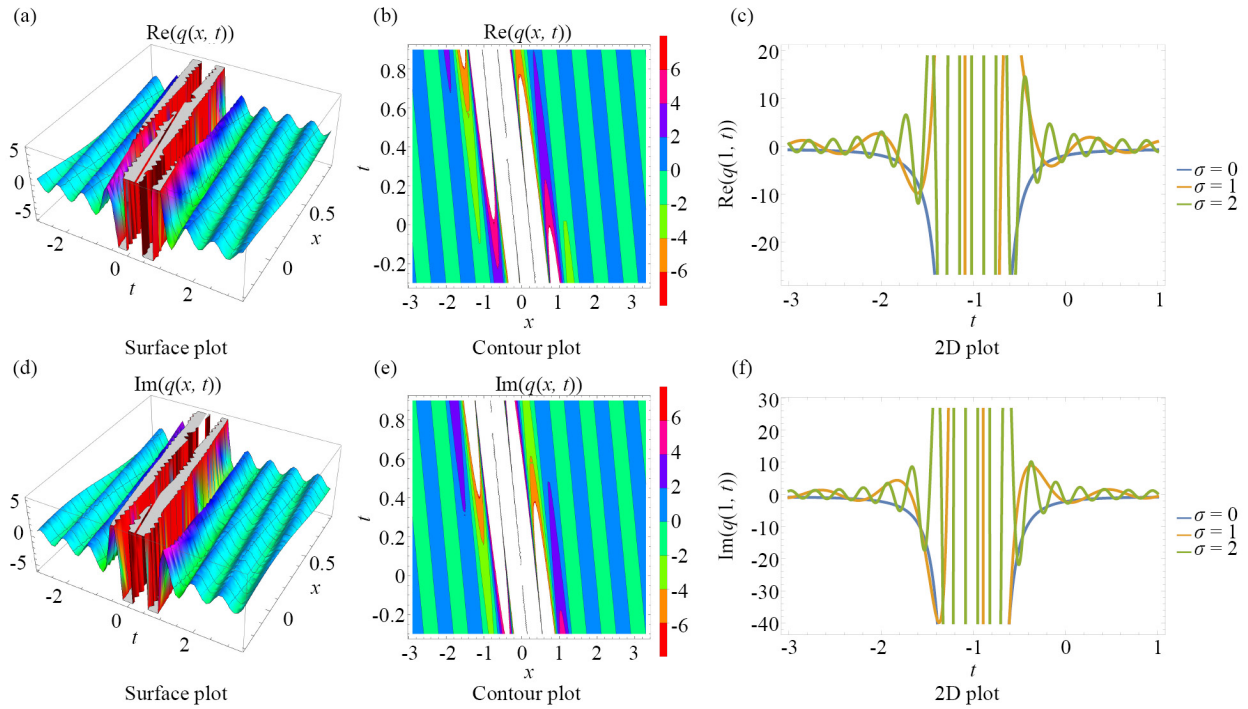

Figure 14. A singular soliton given $\sigma = 2$

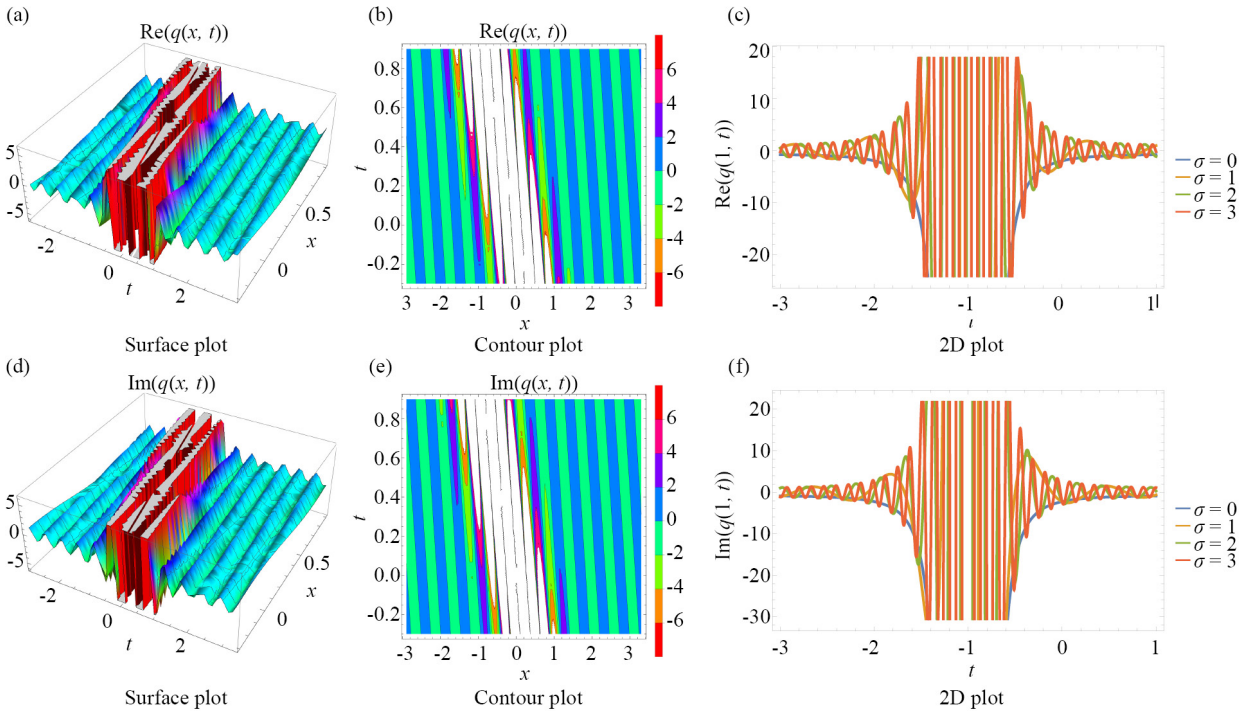

Figure 15. A singular soliton given $\sigma = 3$

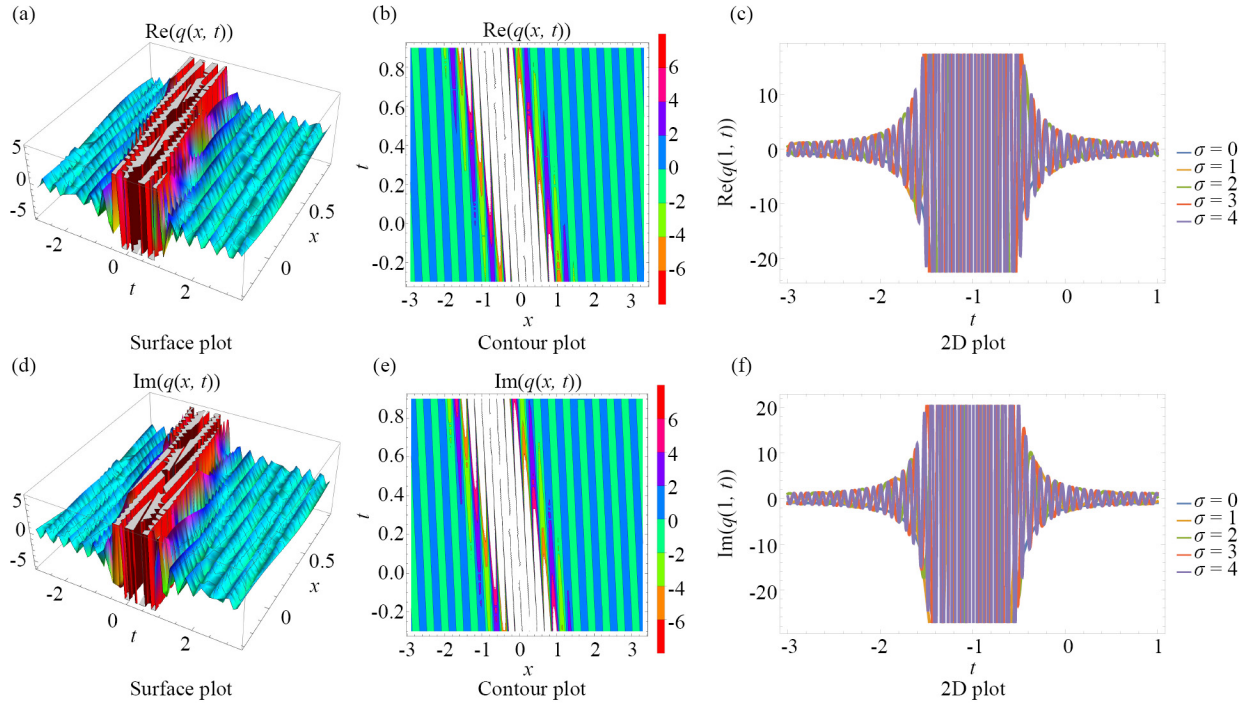

Figure 16. A singular soliton given $\sigma = 4$

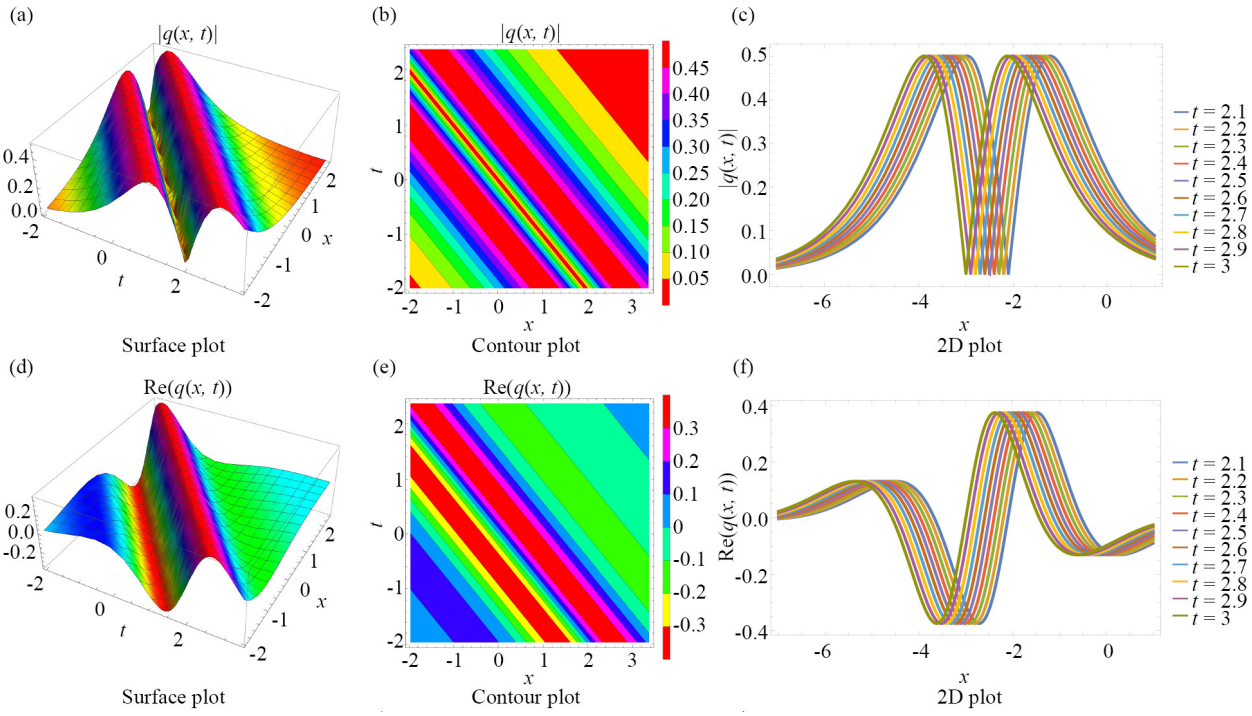

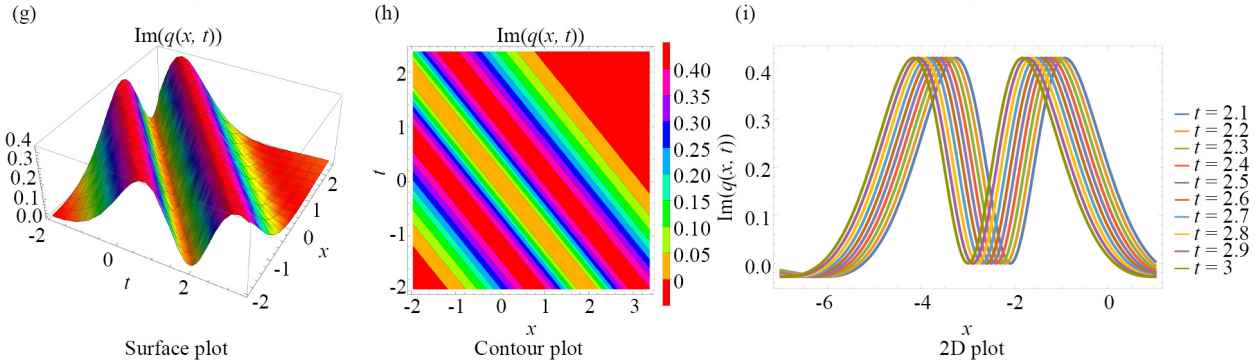

Figure 17. A dark-bright soliton given $\sigma = 0$

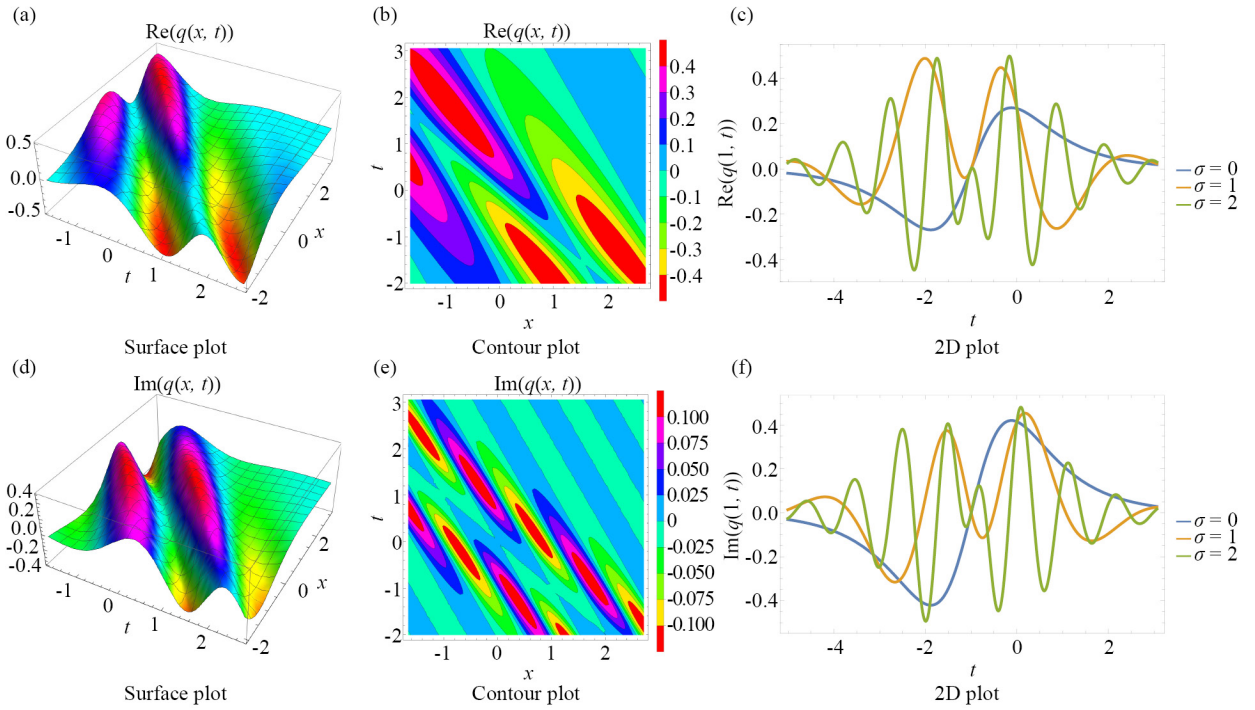

Figure 18. A dark-bright soliton given $\sigma = 2$

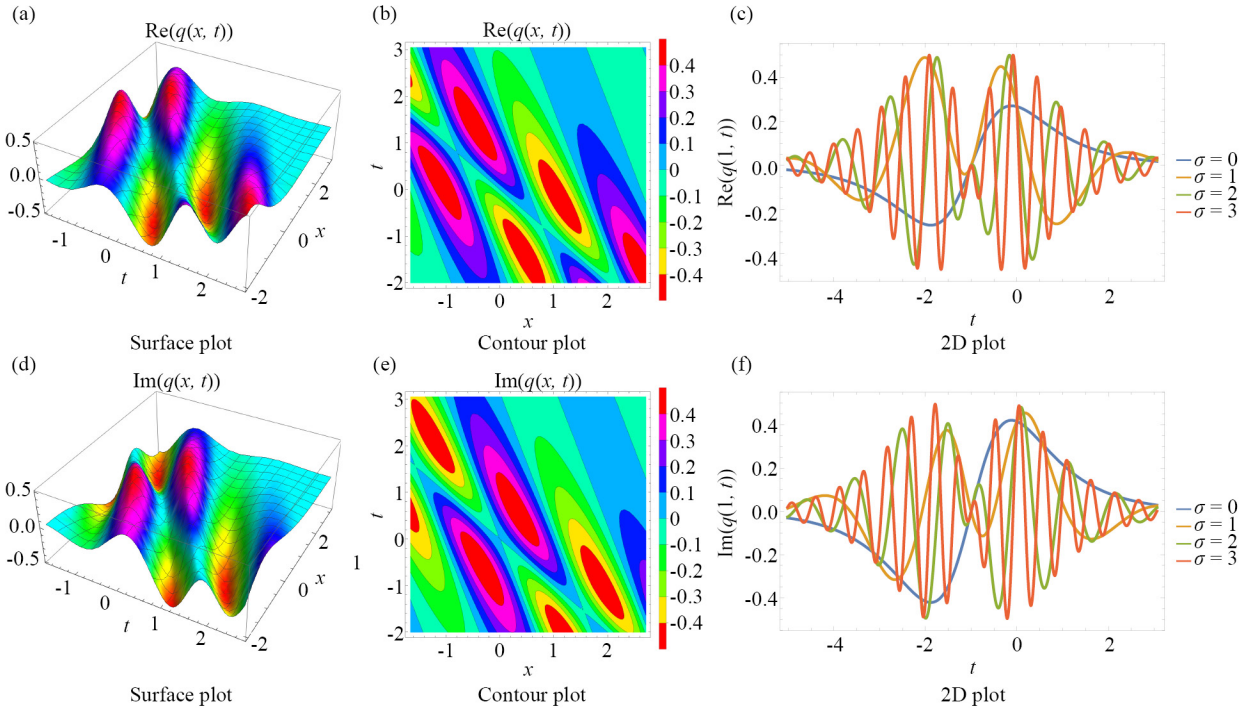

Figure 19. A dark-bright soliton given $\sigma = 3$

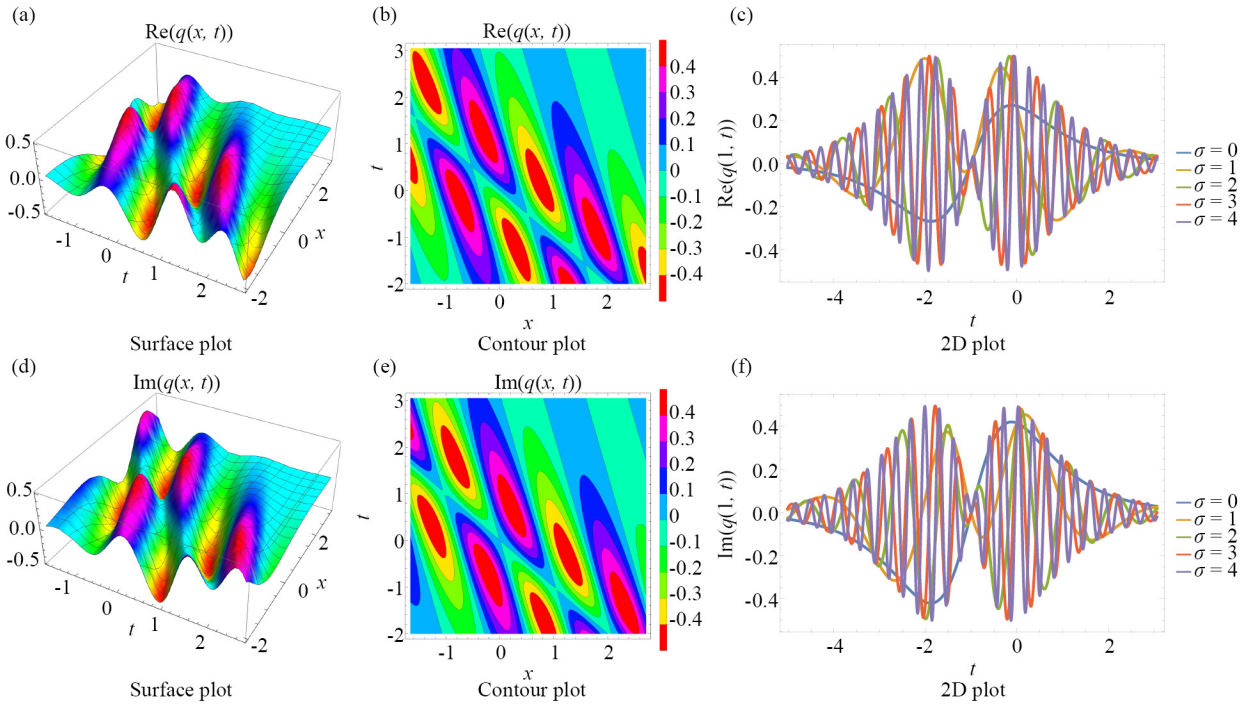

Figure 20. A dark-bright soliton given $\sigma = 4$

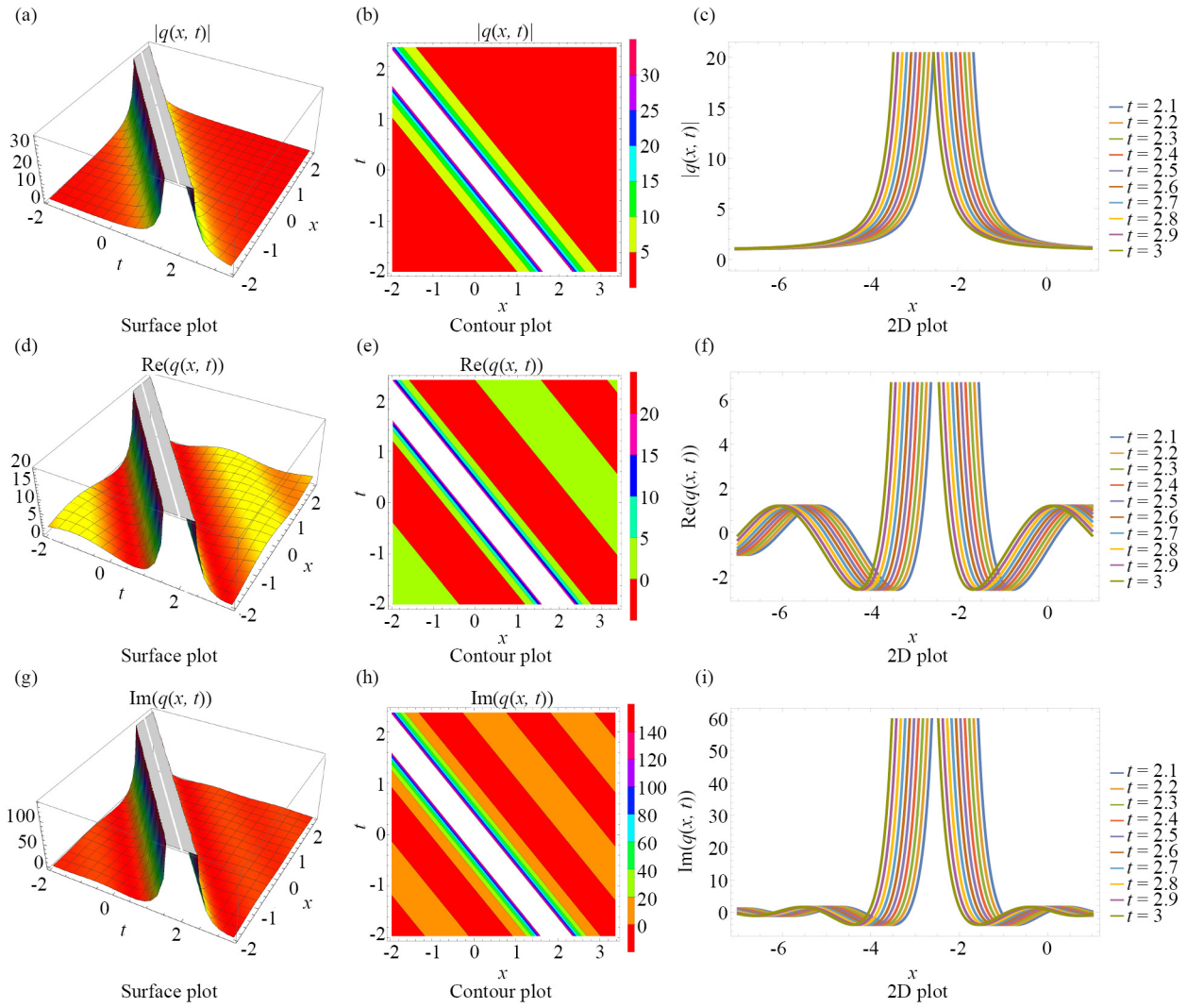

Figure 21. A singular-singular soliton given $\sigma = 0$

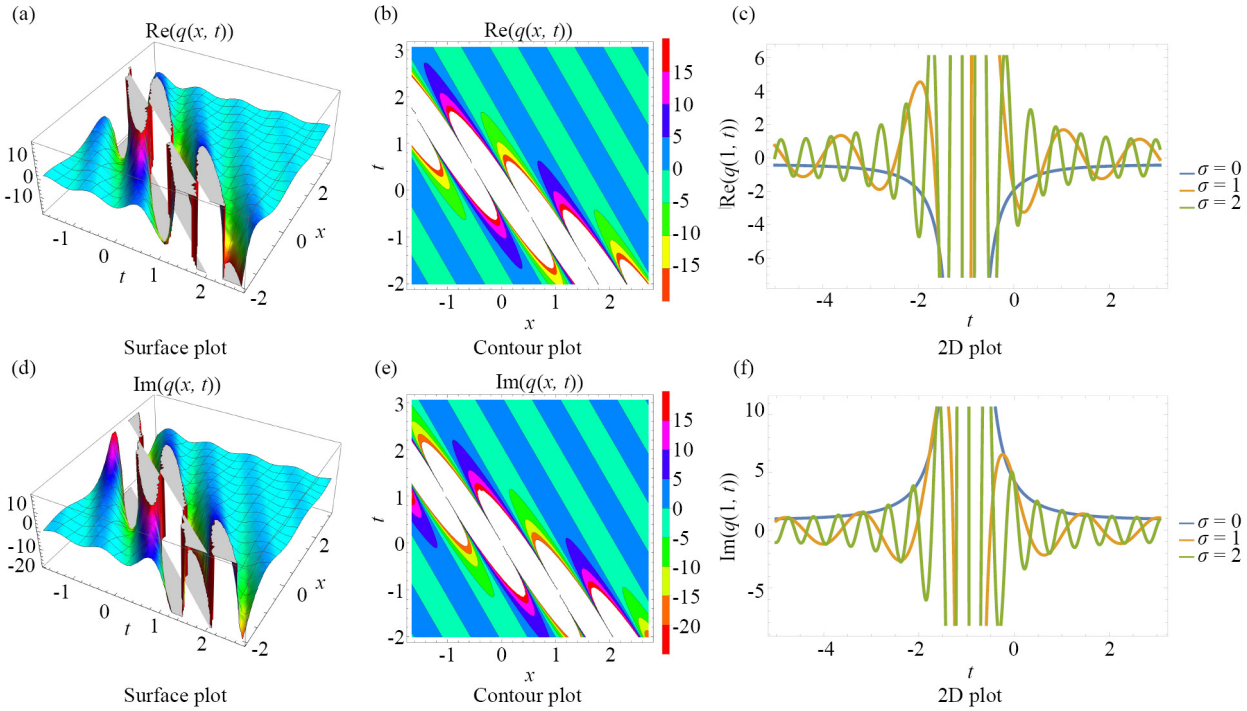

Figure 22. A singular-singular soliton given $\sigma = 2$

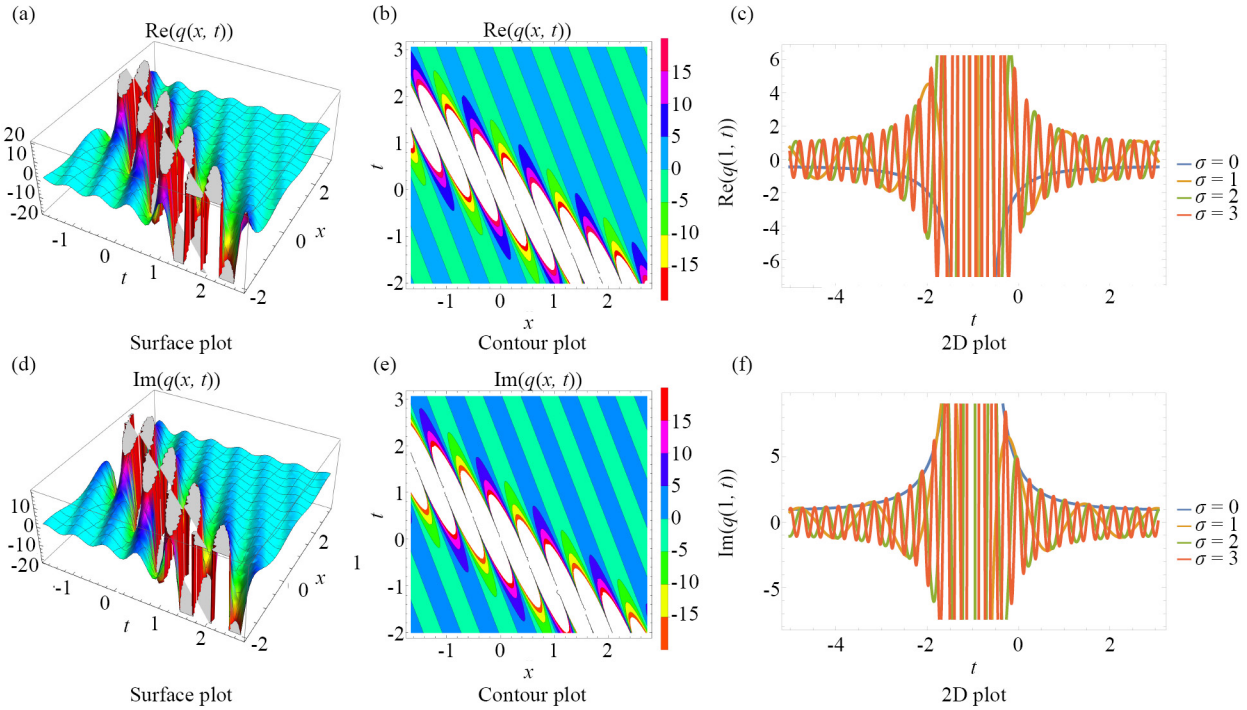

Figure 23. A singular-singular soliton given $\sigma = 3$

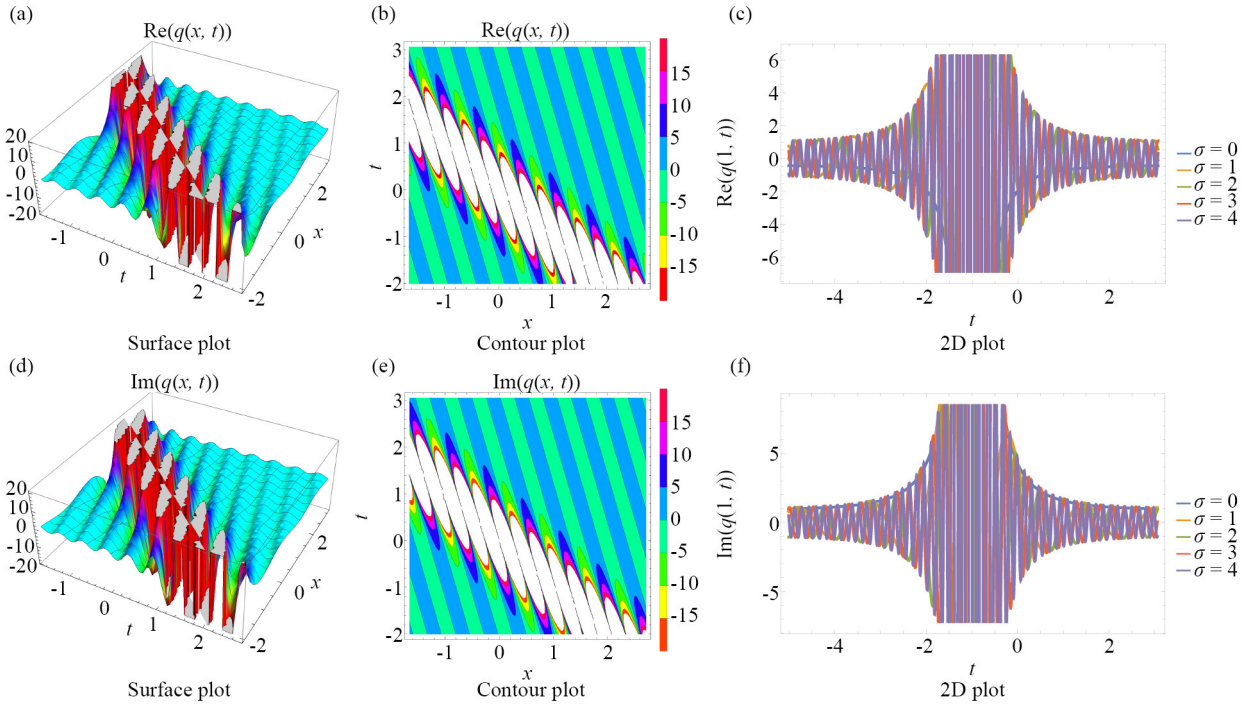

Figure 24. A singular-singular soliton given $\sigma = 4$

The Gaussian nature of the multiplicative white noise introduces significant randomness into the system, influencing the amplitude, phase, and stability of the solitons. This randomness reflects the inherent properties of Gaussian-distributed noise, characterized by a mean of zero and a specified variance. These properties manifest as stochastic fluctuations in soliton dynamics, which are vividly captured in the presented 3D, 2D, and contour plots.

The Gaussian characteristics of the noise directly affect the soliton structures, as evidenced by the graphical results. In the 3D and 2D surface plots, deviations from the ideal deterministic soliton profiles are apparent and can be attributed to the random perturbations introduced by the multiplicative noise. These deviations reflect the system's sensitivity to stochastic influences, where the soliton parameters-such as amplitude and width-undergo noticeable fluctuations. The contour plots further illustrate these effects, linking variations in soliton parameters (height, width, and phase) to the probabilistic nature of the Gaussian noise. These variations correspond to the standard deviation of the Gaussian distribution, effectively visualizing how noise disrupts the soliton's ideal characteristics.

The influence of Gaussian-distributed noise is explicitly demonstrated through multiple realizations of the soliton solutions. By overlaying these realizations in the 3D and 2D plots, the variability in soliton profiles is highlighted, showing the extent to which the soliton structures fluctuate under different noise realizations. Regions of increased deviation in these plots correspond to higher noise intensity, consistent with the expected behavior under Gaussian perturbations. This visualization approach provides a clear understanding of how noise intensity impacts the soliton's stability and coherence, with more pronounced fluctuations occurring as the noise variance increases.

In the contour plots, localized fluctuations in soliton amplitude are particularly prominent. These fluctuations represent areas where the soliton deviates significantly from its deterministic profile, a direct result of the additive effects of Gaussian noise. As the noise intensity increases, these deviations become more pronounced, illustrating the stochastic nature of the system. The probabilistic aspect of the contour plots is further emphasized by the variation in intensity, which reflects the noise-induced perturbations in soliton amplitude and width.

The stochastic variability in soliton parameters is carefully quantified, allowing for a deeper understanding of its physical implications. The amplitude, width, and phase of the solitons exhibit random fluctuations due to the multiplicative white noise, directly affecting their stability and coherence. These effects are not only visualized but also discussed in

terms of their relevance to real-world optical systems, where noise is an unavoidable factor. The analysis reveals that as the noise variance increases, the solitons become less stable, with greater deviations from their ideal profiles. This behavior aligns with theoretical expectations for systems influenced by Gaussian noise and underscores the critical role of stochastic effects in shaping soliton dynamics.

The presented graphs effectively demonstrate the randomness introduced by the Gaussian-distributed noise through multiple realizations of the soliton solutions. These realizations provide a comprehensive picture of the stochastic effects, capturing the variability in soliton dynamics across different noise instances. For instance, in the 3D surface plots, the variability across realizations highlights the perturbations caused by the noise, with regions of increased deviation corresponding to higher noise intensity. Similarly, the contour plots showcase localized fluctuations in soliton amplitude, further reinforcing the connection between noise intensity and soliton behavior.

As a result, the Gaussian-distributed multiplicative white noise plays a pivotal role in shaping the soliton dynamics, introducing fluctuations that are both visually apparent and physically significant. By presenting these stochastic effects through detailed graphical results, we provide valuable insights into the interplay between noise and soliton stability, advancing the understanding of soliton behavior in stochastic systems. These findings lay the groundwork for future studies that can explore more complex noise models and their implications for soliton dynamics.

These figures collectively illustrate the range of behaviors exhibited by different solitons under varying levels of multiplicative white noise. Bright solitons exhibit some resilience, maintaining stability at low noise levels but losing shape as noise increases. Singular solitons, whether standalone or combined, display a high sensitivity to noise, with substantial structural irregularities under noise influence. Dark solitons demonstrate moderate vulnerability, with notable profile disturbances at higher noise levels. The bright-dark soliton solution, with its combination of both soliton types, exhibits complex interactions in response to noise, with both components becoming distorted under increasing σ values. Overall, these results underscore the critical influence of multiplicative white noise on soliton stability and structural integrity, highlighting the importance of accounting for such factors in practical applications where soliton robustness is essential.

6. Conclusion

This study presented a comprehensive analysis of the Gerdjikov-Ivanov equation as applied to soliton dynamics in birefringent optical fibers influenced by multiplicative white noise. The combined effects of birefringence and stochastic perturbations introduced realistic complexity to the system, providing deeper insight into soliton behavior under practical conditions.

Using the enhanced direct algebraic method and the projective Riccati equations method, we derived exact solutions and identified a diverse range of soliton types, including bright, dark, singular, and straddled solitons, along with periodic solutions based on Jacobi and Weierstrass functions. These findings demonstrate the richness of soliton dynamics in complex media and highlight how noise can significantly influence soliton stability and structure.

The analytical techniques and solutions developed here not only deepen the theoretical understanding of nonlinear optical systems but also offer potential applications in designing noise-resilient optical communication systems [33, 34]. Moreover, the methods used can be extended to other nonlinear systems affected by stochastic influences, opening avenues for further interdisciplinary research.

Acknowledgement

One of the authors, Anjan Biswas (AB), is grateful to Grambling State University for the financial support he received as the Endowed Chair of Mathematics. This support is sincerely appreciated.

The authors extend their appreciation to Taif University, Saudi Arabia, for supporting this work through project number (TU-DSPP-2024-46).

Funding

This research was funded by Taif University, Saudi Arabia, Project No. (TU-DSPP-2024-46).

Conflict of interest

The authors claim that there is no conflict of interest.

References

[1] Kruglov VI, Triki H. Propagation of coupled quartic and dipole multi-solitons in optical fibers medium with higher-order dispersions. *Chaos, Solitons & Fractals*. 2023; 172: 113526. Available from: https://doi.org/10.1016/j.chaos.2023.113526.

[2] Zayed EME, Shohib RMA, Alngar MEM. Dispersive optical solitons in birefringent fibers for stochastic Schrödinger-Hirota equation with parabolic law nonlinearity and spatiotemporal dispersion having multiplicative white noise. *Optik*. 2023; 278: 170736. Available from: https://doi.org/10.1016/j.ijleo.2023.170736.

[3] Vega-Guzman J, Biswas A, Mahmood MF, Zhou Q, Khan S, Moshokoa SP. Dark and singular optical solitons in birefringent fibers with Kundu-Eckhaus equation by undetermined coefficients. *Optik*. 2019; 181: 499-502. Available from: https://doi.org/10.1016/j.ijleo.2018.12.080.

[4] Tang L. Bifurcation analysis and multiple solitons in birefringent fibers with coupled Schrödinger-Hirota equation. *Chaos, Solitons & Fractals*. 2022; 161: 112383. Available from: https://doi.org/10.1016/j.chaos.2022.112383.

[5] Menyuk CR. Solitons in birefringent optical fibers and polarization mode dispersion. *Optics Communications*. 2024; 550: 129841. Available from: https://doi.org/10.1016/j.optcom.2023.129841.

[6] Ablowitz MJ, Horikis TP. Rogue waves in birefringent optical fibers: elliptical and isotropic fibers. *Journal of Optics*. 2017; 19(6): 065501. Available from: https://doi.org/10.1088/2040-8986/aa69da.

[7] Choksi N, Qian L. Vector theory of optical nonlinearities in birefringent fibers. *Journal of Lightwave Technology*. 2024; 42(16): 5663-5673. Available from: https://doi.org/10.1109/JLT.2024.3397079.

[8] Akram U, Tang Z, Althobaiti S, Althobaiti A. Dynamics of optical dromions in concatenation model. *Nonlinear Dynamics*. 2024; 112: 14321-14341. Available from: https://doi.org/10.1007/s11071-024-09810-6.

[9] Biswas A. Dynamics of Super-Gaussian solitons in Birefringent optical fibers. *Journal of Nonlinear Optical Physics & Materials*. 2001; 10(1): 29-42. Available from: https://doi.org/10.1142/S0218863501000413.

[10] Zayed EME, Gepreel KA, El-Horbaty M, Arnous AH, Secer A, Ozisik M, et al. Investigating dispersive optical soliton dynamics in birefringent fibers with cubic nonlinearity through quintic-order concatenation model. *Optical Fiber Technology*. 2024; 88: 103957. Available from: https://doi.org/10.1016/j.yofte.2024.103957.

[11] Viscarra MA, Urzagasti D. Dark soliton solutions of the cubic-quintic complex Ginzburg-Landau equation with high-order terms and potential barriers in normal-dispersion fiber lasers. *Journal of Nonlinear Optical Physics & Materials*. 2022; 31(1): 2250003. Available from: https://doi.org/10.1142/S0218863522500035.

[12] Ferreira MFS. Soliton transmission in fibers with Polarization-mode dispersion. *Fiber and Integrated Optics*. 2008; 27(3): 113-126. Available from: https://doi.org/10.1080/01468030802040063.

[13] Khoso IA, Katbar NM, Akram U. Optical dromions for spatiotemporal fractional nonlinear system in quantum mechanics. *Quantum Reports*. 2023; 5(3): 546-564. Available from: https://doi.org/10.3390/quantum5030036.

[14] Akram U, Althobaiti A, Althobaiti S, Alhushaybari A. Chirped pulses for Nematicons in liquid crystals with cubic-septic law nonlinearity. *Chaos, Solitons & Fractals*. 2023; 174: 113842. Available from: https://doi.org/10.1016/j.chaos.2023.113842.

[15] Seadawy AR, Akram U, Rizvi STR. Dispersive optical solitons along with integrability test and one soliton transformation for saturable cubic-quintic nonlinear media with nonlinear dispersion. *Journal of Geometry and Physics*. 2022; 177: 104521. Available from: https://doi.org/10.1016/j.geomphys.2022.104521.

[16] Al-Ghafri KS, Krishnan EV, Biswas A. Cubic-quartic optical soliton perturbation and modulation instability analysis in polarization-controlled fibers for Fokas-Lenells equation. *Journal of the European Optical Society-Rapid Publications*. 2022; 18(2): 9. Available from: https://doi.org/10.1051/jeos/2022008.

[17] Onder I, Secer A, Ozisik M, Bayram M. Obtaining optical soliton solutions of the cubic-quartic Fokas-Lenells equation via three different analytical methods. *Optical and Quantum Electronics*. 2022; 54(12): 786. Available from: https://doi.org/10.1007/s11082-022-04119-3.

[18] Zayed EME, Alngar MEM, Biswas A, Yıldırım Y, Khan S, Alzahrani AK, et al. Cubic-quartic optical soliton perturbation in polarization-preserving fibers with Fokas-Lenells equation. *Optik*. 2021; 234: 166543. Available from: https://doi.org/10.1016/j.ijleo.2021.166543.

[19] Peng C, Li Z. Dynamics and optical solitons in polarization-preserving fibers for the cubic-quartic complex Ginzburg-Landau equation with quadratic-cubic law nonlinearity. *Results in Physics*. 2023; 51: 106615. Available from: https://doi.org/10.1016/j.rinp.2023.106615.

[20] Zayed EME, Shohib RMA, Alngar MEM, Gepreel KA, Nofal TA, Yıldırım Y. Optical solitons for Biswas-Arshed equation with multiplicative noise via Itô calculus using three integration algorithms. *Optik*. 2022; 258: 168847. Available from: https://doi.org/10.1016/j.ijleo.2022.168847.

[21] Yaşar E, Yıldırım Y, Yaşar E. New optical solitons of space-time conformable fractional perturbed Gerdjikov-Ivanov equation by sine-Gordon equation method. *Results in Physics*. 2018; 9: 1666-1672. Available from: https://doi.org/10.1016/j.rinp.2018.04.058.

[22] Tang MY. Exact chirped solutions of the perturbed Gerdjikov-Ivanov equation with spatio-temporal dispersion. *Zeitschrift für Naturforschung A*. 2023; 78(8): 703-719. Available from: https://doi.org/10.1515/zna-2023-0093.

[23] Zulfiqar A, Ahmad J. New optical solutions of conformable fractional perturbed Gerdjikov-Ivanov equation in mathematical nonlinear optics. *Results in Physics*. 2021; 21: 103825. Available from: https://doi.org/10.1016/j.rinp.2021.103825.

[24] Rehman HU, Akber R, Wazwaz AM, Alshehri HM, Osman. Analysis of Brownian motion in stochastic Schrödinger wave equation using Sardar sub-equation method. *Optik*. 2023; 289: 171305. Available from: https://doi.org/10.1016/j.ijleo.2023.171305.

[25] Zulfiqar H, Aashiq A, Tariq KU, Ahmad H, Almohsen B, Aslam M, et al. On the solitonic wave structures and stability analysis of the stochastic nonlinear Schrödinger equation with the impact of multiplicative noise. *Optik*. 2023; 289: 171250. Available from: https://doi.org/10.1016/j.ijleo.2023.171250.

[26] Rehman HU, Iqbal I, Zulfiqar H, Gholami D, Rezazadeh H. Stochastic soliton solutions of conformable nonlinear stochastic systems processed with multiplicative noise. *Physics Letters A*. 2023; 486: 129100. Available from: https://doi.org/10.1016/j.physleta.2023.129100.

[27] Chou D, Rehman HU, Amer A, Amer A. New solitary wave solutions of generalized fractional Tzitzéica-type evolution equations using Sardar sub-equation method. *Optical and Quantum Electronics*. 2023; 55(13): 1148. Available from: https://doi.org/10.1007/s11082-023-05425-0.

[28] Arshed S. Two reliable techniques for the soliton solutions of perturbed Gerdjikov-Ivanov equation. *Optik*. 2018; 164: 93-99. Available from: https://doi.org/10.1016/j.ijleo.2018.02.119.

[29] Kaur L, Wazwaz AM. Optical solitons for perturbed Gerdjikov-Ivanov equation. *Optik*. 2018; 174: 447-451. Available from: https://doi.org/10.1016/j.ijleo.2018.08.072.

[30] Arnous AH, Hashemi MS, Nisar KS, Shakeel M, Ahmad J, Ahmad I, et al. Investigating solitary wave solutions with enhanced algebraic method for new extended Sakovich equations in fluid dynamics. *Results in Physics*. 2024; 57: 107369. Available from: https://doi.org/10.1016/j.rinp.2024.107369.

[31] Arnous AH, Mirzazadeh M, Hashemi MS, Shah NA, Chung JD. Three different integration schemes for finding soliton solutions in the (1 + 1)-dimensional Van der Waals gas system. *Results in Physics*. 2023; 55: 107178. Available from: https://doi.org/10.1016/j.rinp.2023.107178.

[32] Arnous AH, Mirzazadeh M, Akinyemi L, Akbulut A. New solitary waves and exact solutions for the fifth-order nonlinear wave equation using two integration techniques. *Journal of Ocean Engineering and Science*. 2023; 8(5): 475-480. Available from: https://doi.org/10.1016/j.joes.2022.02.012.

[33] Hussain A, Usman M, Zaman F, Zidan AM, Herrera J. Noether and partial Noether approach for the nonlinear (3 + 1)-dimensional elastic wave equations. *PLOS ONE*. 2025; 20(1): e0315505. Available from: https://doi.org/10.1371/journal.pone.0315505.

[34] Zinat N, Hussain A, Kara AH, Zaman FD. Lie group analysis and conservation laws for the time-fractional 3D Bateman-Burgers equation. *Afrika Matematika*. 2025; 36(2): 1-16. Available from: https://doi.org/10.1007/s13370-025-01295-9.